UNIVERSITY OF CALIFORNIA SAN DIEGO

Modeling Mammary Tumor Invasion in Response to Changes in Matrix Stiffness

A Thesis submitted in partial satisfaction of the requirements for the degree of Master of Science

in

Bioengineering

by

Christopher Plunkett

Committee in charge:

Professor Adam Engler, Chair
Professor Stephanie Fraley
Professor Jing Yang

2018

The Thesis of Christopher Plunkett is approved, and it is acceptable in quality and form for publication on microfilm and electronically:

_____

_____

_____
Chair

University of California San Diego

2018

DEDICATION

To my mother and father

TABLE OF CONTENTS

LIST OF FIGURES

ACKNOWLEDGEMENTS

I would like to thank Professor Adam Engler for his mentorship and support throughout the duration of this project. He has been an incredible source of knowledge and assistance for my scientific and career pursuits and I am extremely grateful for the privilege of working with him over the past year. I also thank my committee, Professor Stephanie Fraley, and Professor Jing Yang for their assistance in this process.

I also wish to thank all the members of the Engler lab for their advice, assistance, and friendship during my time here. Every day of work has been an absolute joy because of them. I wish to give special thanks Aditya Kumar for his mentorship and support throughout my time here. His contributions to my work and career are innumerable and it has been an honor to work with him. Finally, I wish to thank the undergraduate students who have worked with me during my time here: Jaime Yastorza, Susan Hou, and Kirsten Wong. Their commitment to this work and excitement for science is truly an inspiration and I have no doubt they will all go on to achieve great things.

Finally, I would not be where I am today without my friends and family. I would like to thank, above all else, my mother and father who, through their teachings, sacrifice, and love, raised me to be the man I am today. I thank them from the bottom of my heart for all they have done.

Chapter 2, in full, is a reprint of the material as it appears in Ondeck M, Kumar A, Placone J, Plunkett C, Matte B, Wong K, Fattet L, Yang J, Engler A. Dynamically Stiffening Niche Promote Malignant Transformation of Mammary Epithelial Cells via Collective Mechanical Signaling. Submitted. The Thesis author was the second author of this paper.

VITA

2016 Bachelor of Science, University of Rochester

2017 Master of Science, University of California San Diego

PUBLICATIONS

Ondeck M[*], Kumar A[*], Placone J[*], **Plunkett C**, Matte B, Wong K, Fattet L, Yang J, Engler A. Dynamically Stiffening Niche Promote Malignant Transformation of Mammary Epithelial Cells via Collective Mechanical Signaling. Submitted. * denotes co-author

FIELDS OF STUDY

Major Field: Bioengineering

Studies in Mechanobiology
Professor Adam Engler

ABSTRACT OF THE THESIS

Modeling Mammary Tumor Invasion in Response to Changes in Matrix Stiffness

by

Christopher Plunkett

Master of Sciences in Bioengineering

University of California San Diego, 2018

Professor Adam J. Engler, Chair

The progression of mammary carcinoma involves a variety of cellular and environmental factors that facilitate invasion of the stroma. Stiffening of the extracellular matrix is associated with increased proliferation and migration of mammary epithelial cells (MECs). Adding further complexity, the MEC microenvironment is dynamic, stiffening nearly 40-fold gradually as the stroma remodels from normal stiffness of ~150 Pascals

to ~5700 Pascals (Pa). These environmental changes occur alongside the emergence of aggressive cellular subpopulations within the tumor mass whose sensitivity to ECM stiffness may vary dramatically.

To mimic stiffening of the tumor microenvironment, we utilized a methacrylated hyaluronic acid hydrogel that could be stiffened in the presence of cells. MCF10A organoids cultured on this substrate showed partial loss of their ductal phenotype in response to stiffening. Activation of TGF-β and YAP signaling was observed and dual inhibition of these pathways significantly reduced the number of invasive cells per organoid. We then sought to determine whether malignant subpopulations within a tumor could alter the mass' stiffness sensitivity. MECs were cultured on polyacrylamide gels ranging from normal mammary stiffness, ~150 Pa, to malignant and stiff, ~5700 Pa. H-Ras transformed cells spread at 150 Pa. with their invasive fraction adopting mesenchymal-like morphology, disruption of E-Cadherin, reduced basement membrane, and nuclear localization of the EMT transcription factor Twist1. Stiffness-mediated transformation was blocked by treatment with R-Roscovitine, suggesting an important link between stiffness sensitivity and intercellular CDK activity. These data demonstrate a complex relationship between ECM stiffness, mutational status, and invasive potential in MECs.

Chapter 1.

Introduction

1.1 Introduction

Mammary carcinoma is the most prevalent cancer among women and accounted for over 250,000 reported cases in 2017[1]. While public awareness, increases in mammograms and early detection, and developing therapies such as immuno-oncology have helped lower mortality rate of the disease to roughly 14% of diagnosed cases, it remains the second most common cancer related cause of death in women[2, 3]. Metastasis, or the emergence of secondary malignancies separate from the primary tumor, is largely responsible for these remaining mortalities. The presence of distal metastases to the bone, liver/lung, or other soft tissues correlates with a drop in five year survival rate of nearly 75%[4]. Treatment options at this stage are oriented largely around chemotherapy and endocrine therapy both of which provide limited efficacy long term and, in the case of chemotherapy, result in extreme negative side effects and reductions in quality of life[5]. Thus the development of therapeutic strategies to combat metastasis poses a highly significant opportunity to reduce fatalities associated with mammary carcinomas.

Molecular and biochemical mechanisms for metastatic progression have been thoroughly investigated as a direct means for inhibition of cellular invasion[6-8]. Among these proposed mechanisms, the epithelial to mesenchymal transition (EMT), a developmental pathway associated with loss of tissue organization and increases in invasive potential has garnered particular interest due to its apparent activation in many

metastatic cell populations[9]. As a result therapeutic strategies targeting key EMT activators such as TGF-β have begun to emerge in clinical trials[10, 11]. In addition to biological mechanisms, physical stimuli have been found to play an increasingly important role in cell behavior[12, 13]. The rise of hydrogel based model systems to probe environmental cues such as extracellular matrix stiffness, viscoelasticity, porosity, and composition have yielded many exciting new mechanisms for cancer cell progression, migration, and proliferation[14]. Such systems lend themselves especially well to ductal carcinomas as the culture of mammary acini *in vitro* has been well established on these substrates[15-18].

In this introductory section, I will provide an overview of the state of these fields of study in order to provide appropriate context to the subsequent work. To do this, I will first outline the metastatic progression as it is currently understood within the ductal subtype of breast cancer and how the transition of cells from an epithelial to mesenchymal phenotype can induce hallmark metastatic behavior in mammary carcinoma. Next, I will characterize how environmental cues, and specifically stiffness of the extracellular matrix, can alter cell behavior and promote an invasive, mesenchymal like phenotype. Finally, I will describe some of the challenges and remaining unknowns facing this field of study and how emerging technologies may offer solutions moving forward.

1.2 Breast Cancer Metastasis and the Epithelial to Mesenchymal Transition

1.2.1 Clinical and Phenotypic Characteristics of Ductal Carcinoma Metastasis

Ductal carcinoma, as the name implies, is a malignancy of the mammary gland's ductal epithelium[19, 20]. As it is currently understood, the progression of this disease begins with the emergence of an atypical hyperplasia of the epithelium which begins to obstruct the luminal space. This outgrowth will then progress into a ductal carcinoma *in situ* (DCIS) which constitutes a full obstruction of the lumen and is clinically defined as a "Stage 0" carcinoma. Left untreated, this DCIS may begin to expand beyond the confines of the mammary duct resulting in an invasive ductal carcinoma[21, 22]. At this point, the tumor is assigned a classification of "Stage 1" and will rise in grade as tumor size and invasion to the surrounding lymph nodes increases. Distally metastatic tumors where cells haves spread beyond the mammary stroma and lymph nodes (e.g. to the liver, lungs, brain, and bone) is assigned a grade of "Stage 4", requires the most aggressive treatment regimens, and is associated with extremely poor prognosis.

The transition from Stage 0 to Stage 4 cancer revolves around the concept of metastasis, or the spreading of cancer to other tissues or organs in the body[23, 24]. The progression toward a fully metastatic cancer begins with the invasion of tumor cells into the surrounding stromal environment and subsequent migration and proliferation within that niche. Eventually, upon reaching the endothelial lining of lymph or blood vasculature, these cells may then enter circulation through intravasation. Following the exit from circulation back through the endothelium or extravasation, tumor cells are then able to form secondary malignancies in peripheral tissues allowing the cancer to spread throughout the body.

1.2.2 Epithelial to Mesenchymal Transition and Metastatic Carcinoma

The absolute dependence of metastatic behavior on localized spreading from the tumor mass has generated considerable interest in the mechanism by which cells exit the ductal environment and proceed to migrate and proliferate in the stroma[25]. This transformation has thusly been thoroughly studied and found to involve, among other features, the loss of polarization, loss of epithelial junctions, reductions or ruptures in ductal basement membrane formation, and increases in the migratory and proliferative capacity of affected cells. These observations suggest that invasive tumor cells may be undergoing an epithelial to mesenchymal transition (EMT) which is an established reprograming of cell phenotype meant to promote injury repair and aid in development[26, 27]. Within a cellular niche, EMT can be induced by soluble factors such as transforming growth factor-β (TGF-β) as well as activation of Wnt, Notch, and RTK mediated signaling pathways[28-31]. These can in turn activate key transcription factors such as Snail, Slug, Zeb1, Zeb2, Twist, and E47 which leads to associated downstream changes such as adherans junction, upregulation of intermediate filaments such as vimentin, and cell polarity loss[32-35].

Extensive evidence for the emergence of EMT in migrating tumor cells has been noted. The critical role of E-cadherin expression in maintaining a healthy, non-cancerous microenvironment has been well established in multiple cancers including breast. Even a partial loss of E-cadherin can drastically alter the malignancy and invasive potential of a given tumor[36-39]. Upregulation of vimentin has also been linked to increased migration in breast cells particularly when coupled with mutation of the H-Ras oncoprotein[40, 41]. More recently, upregulation of EMT markers have been associated with CD44 expressing subpopulations of mammary epithelial cells suggesting a link between EMT and the

proposed cancer stem cell[42-44]. Given these findings, it appears that EMT plays a major role in determining the invasive potential of tumor cells and, therefore, is of great importance in slowing or halting tumor metastasis and, by extension, improving the overall survival rate of breast cancer patients.

1.3 Cancer and Substrate Stiffness

1.3.1 Cellular Response to Environmental Stiffness Cues

Cells are highly sensitive to environmental cues and are constantly responding to changes taking place in their niche. Mechanotransduction, or the cellular sensation of and response to mechanical loading, is one such method by which cells are able to adapt to these cues[12]. There are several examples of mechanotransduction's role in cellular organization. Bone density and shape is highly dependent on mechanical forces applied to the body while vascular wall thickness is determined in part by experienced shear stress and pressure[45-47]. Mechanotransduction is not, however, only mediated by gross mechanical loads placed on the body. Substrate stiffness, transduced by the cellular cytoskeleton through focal adhesions, is also capable of modulating individual cell behavior and phenotype. These signals are often caused by the organization and composition of the extracellular matrix (ECM) which is the heterogeneous aggregate of structural proteins in which cells reside within a tissue. Relative protein composition (e.g. upregulated fibular collagens and fibronectin) as well as organizational differences allow for modulation of ECM stiffness[48-50]. These differences can aid in growth and development by directing cell behavior and fate. For example, mesenchymal stem cells undergoing distinct differentiation to neural, muscular, and bone lineages depending on their culture

substrate stiffness[51]. This cellular sensitivity to ECM stiffness and the subsequent behavioral changes are of particular interest within the study of cancer as the tumor microenvironment is among the most dynamic within the adult human body.

1.3.2 Stiffness and the Breast Cancer Microenvironment

Tumor development is associated with drastic remodeling of the local microenvironment. Partial fibrotic transformation has been observed in the environment of breast tumors ushered in by upregulated MMP activation and conversion of collagen fibers to types I and II[52-54]. Increases in lysyl oxidase crosslinking of collagen and fiber alignment have also been observed with the latter being predictor of negative outcomes in patients[55-57]. Increases in fibronectin and hyaluronan concentration within the local ECM have also been noted[58, 59]. The net result of these changes is an overall increase in the substrate stiffness of tumorigenic mammary tissue[60]. These changes are clinically relevant and fundamental to diagnosis. Mammary tumors are commonly discovered through manual palpation: the presence of a stiff "lump" is often the first sign of a malignant growth[61]. Thus it is unsurprising that such a drastic change in niche stiffness correlates with drastic changes in cell behavior.

The role of stiffness signaling in determining metastatic potential has been documented in breast cancer. Mammary epithelial cells, when cultured on soft substrates, for polarized ductal acini with intact basement membrane while these same cells, when cultured on stiff substrates, spread and proliferate with no defined microarchitecture[14]. Stiffness cues may also play a prominent role in the activation of EMT. The transcription factor Twist1 which is among the key bHLH activators of EMT was found to be activated by increased substrate stiffness in mammary epithelial cells leading to mesenchymal

behavior and increased cellular invasion[62]. Additional mechano-sensors can also play a role in promoting invasive behavior. The transcriptional co-activator YAP is highly mechanosensitive localizing to the nucleus in response to increased cytoskeletal tension[63]. YAP activation is also correlated with cell survival, prevention of anoikis, increased cell plasticity, tumor growth and high motility suggesting it may play a mediating role in transforming stiffness signals into invasive behaviors[64]. Taken together, these findings suggest a critical role for environmental stiffens cues in determining a tumor's invasive potential with pathologically stiff substrates leading to increased motility, proliferation, EMT activation, and metastatic potential.

1.4 Conclusion

Genetic and proteomic changes within tumor cells coupled with environmental remodeling and niche stiffening present a complicated interplay of behaviors within a tumor population. Furthermore, the study of these mechanisms through *in vivo* modeling of the tumor microenvironment is limited by high variability between organisms and challenges associated with cellular isolation and analysis. Fortunately, the use of biomaterials whose mechanical properties can be tightly controlled provides a powerful tool for systematically assessing the contributions of these factors toward metastatic potential. When coupled with artificial mammary organoids whose cellular composition is also pre-determined, this system provides an excellent *in vitro* model for tumor progression. In this Thesis, I will explore two novel uses for these model systems in studying the joint roles of tumor heterogeneity and stiffness changes on tumor invasion. In Chapter 2, I will describe how dynamic stiffness changes (i.e. the transformation from soft

to stiff microenvironment) can promote partial invasive behavior on otherwise benign mammary epithelial cells. In Chapter 3, I will examine how increasing malignancy and the accumulation of oncogenic mutations may increase stiffness sensitivity of mammary tumors. Finally, in Chapter 4, I will summarize the broad impacts of this work and propose future aims to expand upon these findings.

Chapter 2.

Dynamically stiffening niche promote malignant transformation of mammary epithelial cells via collective mechanical signaling

2.1 Abstract

Breast cancer fibrosis is a dynamic process that results in tissue stiffness increasing from normal to malignant over months to years. To more accurately mimic the onset of tumor-associated fibrosis versus conventional static hydrogels, mammary epithelial cells (MECs) were cultured on methacrylated-hyaluronic acid hydrogels, whose stiffness can be dynamically modulated from "normal" (<150 Pascals) to "malignant" (>3000 Pascals), utilizing two-stage polymerization. MECs form and remain as polarized acini but begin to decompose and resemble mesenchymal morphology upon matrix stiffening. However, both the degree of matrix stiffening and culture time prior to stiffening play a large role in acinar transformation as, in both cases, a subset of acini remained insensitive to local matrix stiffness. Acini transformation depended neither on colony size nor cell density and MECs did not exhibit "memory" of prior niche when serially cultured through cycles of soft and stiff matrix. Instead the transcription factor Twist, transforming growth factor β

(TGFβ), and YAP activation appeared to modulate stiffness-mediated signaling; when stiffness-mediated signals were blocked, collective MEC transformation was reduced in favor of single MECs transforming and migrating away from acini. These data indicates a more complex interplay of time-dependent stiffness signaling, acinar structure, and soluble cues that regulate MEC transformation than previous models suggest.

2.2 Introduction

Tissue remodeling results in part from mechanical, structural, and compositional changes to the extracellular matrix (ECM)–the scaffold that surrounds and separates cells. Significant focus over the last decade has illustrated how one such property–ECM stiffness–effects a range of cell behaviors from migration[65] to alignment and morphology[66-68] to differentiation.[51, 69, 70] Yet the remodeling that induces these changes can occur for a number of reasons; for mammary cancers in particular, tumors "feel" stiffer during manual palpation[61] in part from increased ECM expression and crosslinking[60, 71] as well as changes in protein composition.[72-74] This dynamic tumor microenvironment is established by tumor and stromal cells and their soluble factors[75-78] which evolve as the tumor progresses over months to years.[61] Animal models largely recapitulate the dynamics of human tumors, e.g. stiffening by lysyl oxidase-mediated crosslinking,[60] but they remain exceedingly complex. Reductionist approaches using biological and synthetic materials have only recently been available to systematically modulate physical properties over a pathologically relevant range. These materials recreate the classic mesenchymal transformation of mammary epithelial cells (MECs) via changes in stromal stiffness.[14, 79, 80] Yet these materials, especially synthetic ones, often cannot be remodeled by cells *in vitro* and remain static with

time, unlike highly dynamic mammary tissue that undergoes a 10 to 20-fold stiffening during tumor progression.[14, 81]

Recent material advances have created dynamic or "on-demand" systems where crosslinking is temporally regulated to achieve continuous or step-wise crosslinking or degradation that more closely resembles *in vivo* tissue dynamics. Systems often rely on thermal- or photo-activated, pH, enzymatic, or diffusion-based mechanisms;[82] for example, gold nanorod-carrying liposomes can be heated past their transition temperature to induce rupture and, when loaded with calcium, form additional alginate crosslinks.[83] Alternatively, thermal sensitive polymers such as N-isopropyl acrylamide undergo substantial shape changes when heated, resulting in changes in mesh size and stiffness of their hydrogels.[84] Large thermal changes may be detrimental to cells, so light, which can be precisely controlled over space and time, serves as an alternative. Both ultraviolet light (UV) activated crosslinking via radical polymerization[85-88] or degradation via *o*-nitro benzyl groups[89] have been used to modulate cell behavior, finding that stem cells can dynamically modulate their lineage initially[85] but commit after long-term culture.[51, 90] Similar "memory" may exist in cancer cells,[91] prompting the question of whether MECs, which form hollow 3D structures called acini *in vivo*, exhibit single or collective cell behavior when cultured in dynamically stiffening materials. These systems also better mimic how the microenvironment is modified over time with tumors versus static materials, enabling us to additionally determine when and to what extent acini are sensitive to ECM stiffness.

2.3 Results

2.3.1 Methacrylated hyaluronic acid hydrogels recapitulate mammary morphogenesis

Dynamic changes in matrix stiffness–not just stiffness itself[14]–may play a pivotal role in regulating epithelial to mesenchymal transition (EMT), a process where MECs adopt a more mesenchymal-like phenotype punctuated by expression of canonical mesenchymal transcription factors including Twist.[35] To examine the collective responses of 3D acini to stiffening, we adopted a material-based strategy where the methacrylated glycosaminoglycan hyaluronic acid (MeHA) would be partially crosslinked, cells seeded on its collagen-functionalized surface, and Matrigel overlaid on top (Supplementary Fig. 1) consistent with previous methods that used static materials.[134] MeHA has a stiffness range that spans normal to pathologically stiff (Fig. 1A) and could be modulated by the methacrylation substitution ratio, which ranged from 35-50%, free radical donor concentration, which was controlled by UV-activated Irgacure 2959 and UV exposure time.[92] Collagen can be covalently attached to MeHA (Fig. 1B) to a degree similar to polyacrylamide hydrogels as assessed by how tethered the matrix protein is to the substrate.[93]

Initial MEC attachment did not vary as a function of stiffness or substrate (Fig. 1C) and MeHA, stiffened only to initially polymerize it, yielded MEC responses consistent with previous static results on polyacrylamide hydrogels;[14] pathologically stiff cultures induce EMT whereas physiological soft cultures do not (Fig. 1D-E).

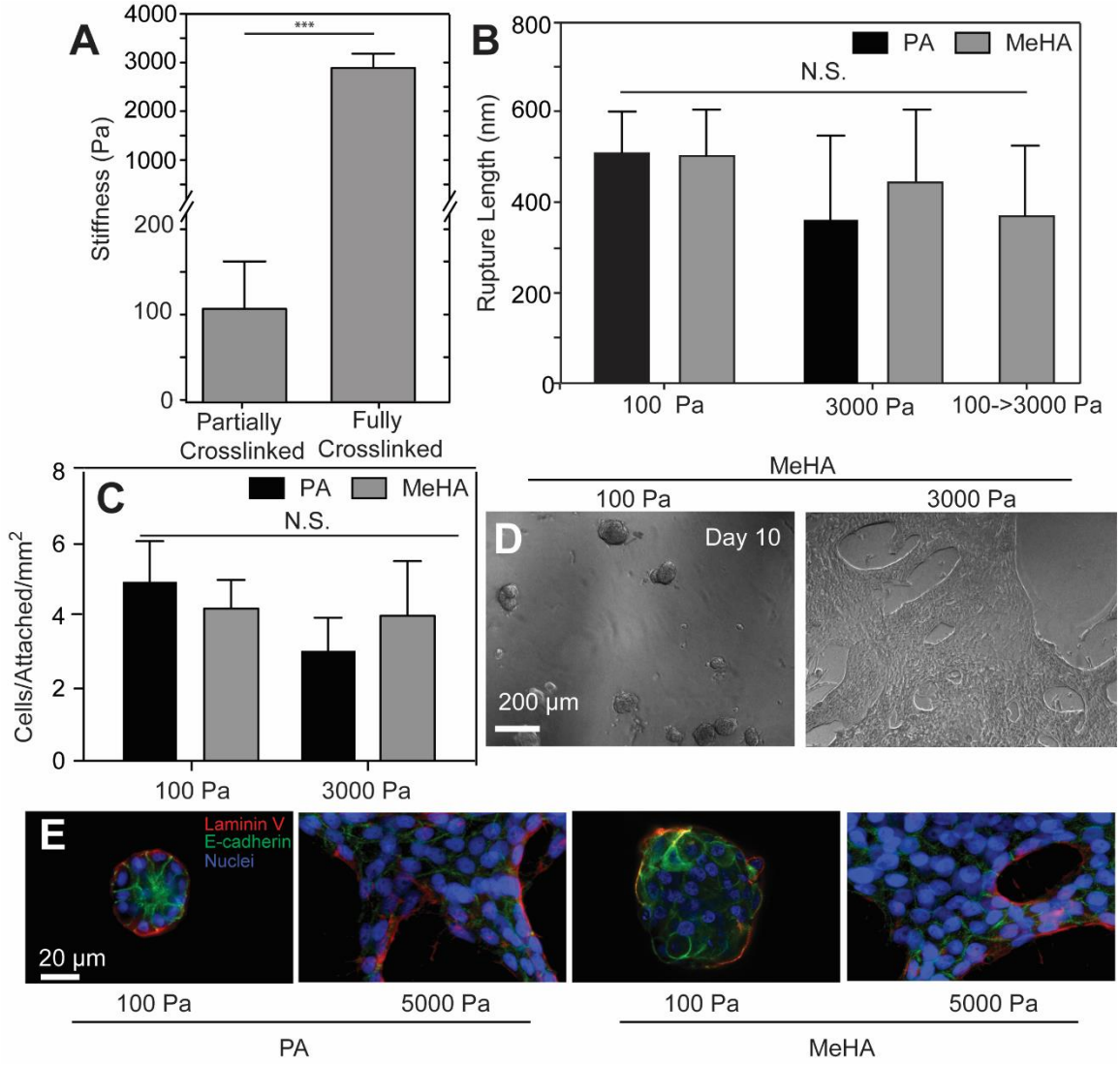

Figure 2.1. Tunable MeHA hydrogels have similar properties to PA hydrogels.
MeHA stiffness is plotted for hydrogels that were crosslinked in a two-stage process.[92] (A) For each batch of MeHA, hydrogel crosslinking time was adjusted to achieve these target values unless otherwise noted. Data here represent mean ± standard deviation for triplicate polymerization from first batch of MeHA (n>100 measurements over multiple gels/bar). ***$p<10^{-3}$ from an unpaired student t-test. (B) Type I collagen attachment is shown by rupture length of the tether pulled off of the surface as in Wen et al.[144] to assess how protein-hydrogel coupling. No statistical difference by two-way ANOVA was found between 100 Pa and 3000 Pa hydrogels fabricated using MeHA or PA as well as MeHA hydrogels that were stiffened using the two-stage process (n>100 measurements over 3 independent gels/bar). (C) Initial MEC attachment is plotted as a function of stiffness or substrate. No statistical difference by two-way ANOVA was found (n = 3 hydrogels containing over 50 cells/bar). (D) Phase images demonstrating MCF10A cell response on 100 and 3000 Pa MeHA substrates 10 days post seeding. Scale bar is 200 µm. (E) Fluorescent images of E-cadherin (green), Laminin V (red), and nuclei (blue) for both 100 and 3000 Pa substrates made using either polyacrylamide (PA) or MeHA as indicated and which are consistent with previous PA hydrogel studies.[14, 79]

2.3.2 Acinus EMT depends on magnitude and timing of substrate stiffening

Via static culture, single MECs undergo EMT and form a layer of mesenchymal cells above 400 Pa or >2-fold above normal ECM stiffness.[134] To determine to what extent MECs are sensitive collectively to ECM stiffness as acini, single cells were cultured on 100 Pa MeHA hydrogels to form acini and then stiffened to varying degrees after 10 days (Fig. 2A). Stiffening up to 3000 Pa requires the presence of both a free radical donor and UV light (Supplementary Fig. 2) up to 2.5 minutes, which was not sufficient to induce DNA damage pathways, e.g. p53 activation (Supplemental Fig. 3); these data suggest that MEC responses are stiffness-mediated and not the result of MeHA polymerization chemistry. After substrates where stiffened to 1000 to 5000 Pa (Fig. 2A), we found that collective MEC responses were still stiffness-dependent; fewer acini maintained their spheroid morphology on 5000 vs. 1000 Pa hydrogels, often exhibiting significant migration away from the original acinus (Fig. 2B). However, cell responses were notably heterogeneous at intermediate stiffness; despite 10-fold change in stiffness, 50% of acini maintained their morphology when MeHA hydrogels were stiffened from 100 to 1000 Pa. Conversely, relatively few acini remained when MeHA was stiffened to pathological stiffness (Fig. 2C). These data suggest that the heterogeneity of tumor progression may be due in part to different sensitivities of a collective MEC response to stroma stiffness changes.

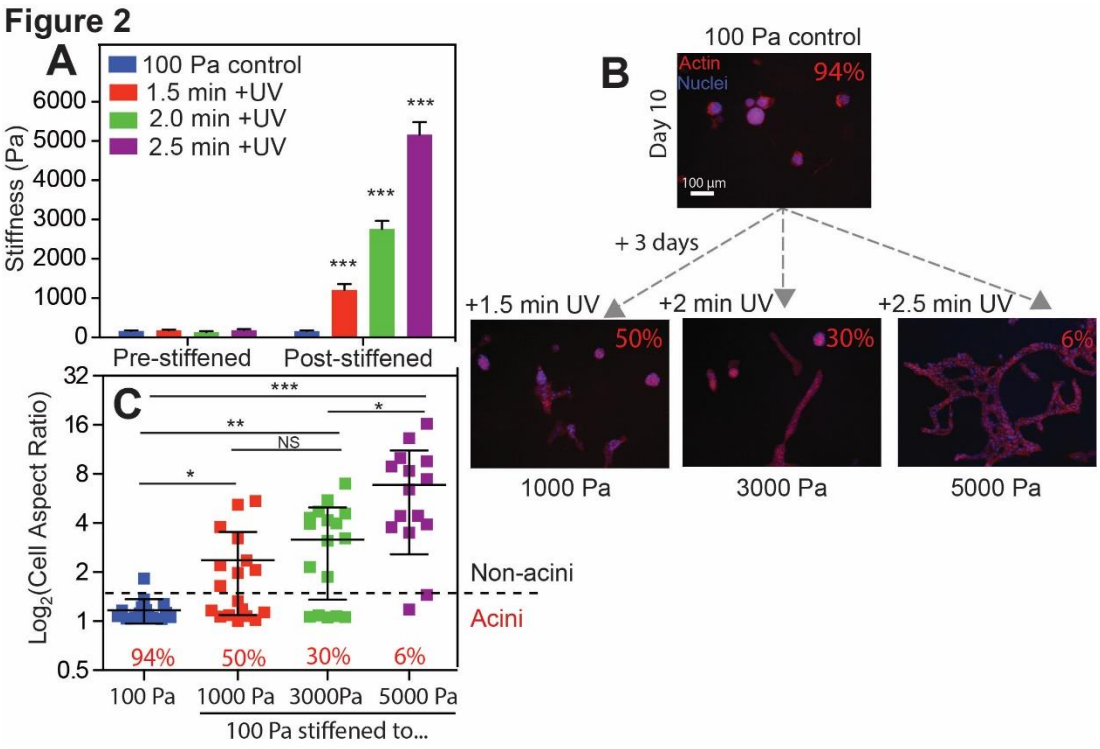

Figure 2.2. MeHA substrates have tunable stiffness to interrogate MEC response to dynamic stiffening
(A) Hydrogel stiffness was measured using AFM for substrates after the initial polymerization step (pre-stiffened) and then after the second polymerization step (post-stiffened). Each color corresponds to a different UV duration in the presence of the Irgacure 2959 photoinitiator (n=6 hydrogels with >20 measurements per gel/bar). ***$p<10^{-3}$ from a paired student t-test between the pre- and post-stiffened states of each substrate. (B) MECs were cultured as indicated and stained for actin (red) and nuclei (blue). (C) Images pre- and post-stiffening MEC morphology were assessed for the three UV exposure periods, i.e. 1000, 3000, and 5000 Pa hydrogels. Cell aspect ratio is plotted with each color corresponding to the stiffening regiment in panel A. The dashed line at 1.5 indicates an approximate transition point from acinar to non-acinar morphology (aspect ratio of 1 indicate a perfect spherical projection) and percentage of data below the transition is shown. *$p<0.05$, **$p<10^{-2}$, and ***$p<10^{-3}$ from an unpaired student t-test (n>15 acini/condition).

The onset of collective stiffness sensitivity is also not clear, so we next varied MEC culture time before stiffening MeHA substrates to the same degree (Fig. 3A). With increased culture time on physiological stiffness, MECs matured into acini (Fig. 3B, left) whereas MECs on pathologically stiff substrates exhibited spreading, proliferation, and morphological changes indicative of EMT-like behavior as early as 2 days in culture (Fig. 3B, right). However when stiffened to 3000 Pa after a variable amount of pre-culture time at 100 Pa, we found that collective MEC responses became heterogeneous after 8 to 10

days of pre-culture; a subset of acini ~10-20% did not respond to stiffening by exhibiting EMT-like behavior (Fig. 3B, center; Fig. 3C), suggesting that after sufficient time in culture, acini may have matured to the point where collective sensing among cells within the acinus could override mechanotransductive signals that would induce EMT for those cells in contact with the MeHA.[101] However MECs proliferate[127] and acini hollow[145] as they mature, so the number of cells present in an acinus may regulate their collective sensing. To produce acini of consistent size, MECs were pre-clustered at different densities using Aggrewell plates. After seeding overnight on MeHA, hydrogels were stiffened and acini cultured for up to 5 days (Fig. 4A). However, acinar behavior appeared independent of cell density as it did not affect the propensity of MECs to respond to stiffness; indeed, responses were primarily controlled by stiffness. When MeHA was stiffened, we further observed a decrease in acini in favor of MECs undergoing EMT-like changes (Fig. 4B-E), although we again observed that a subset of acini are insensitive to stiffening (Fig. 4B, D arrowheads, middle row). Together these data suggest that beyond a minimum size or maturity, collective MEC responses to stroma stiffness changes can be heterogeneous.

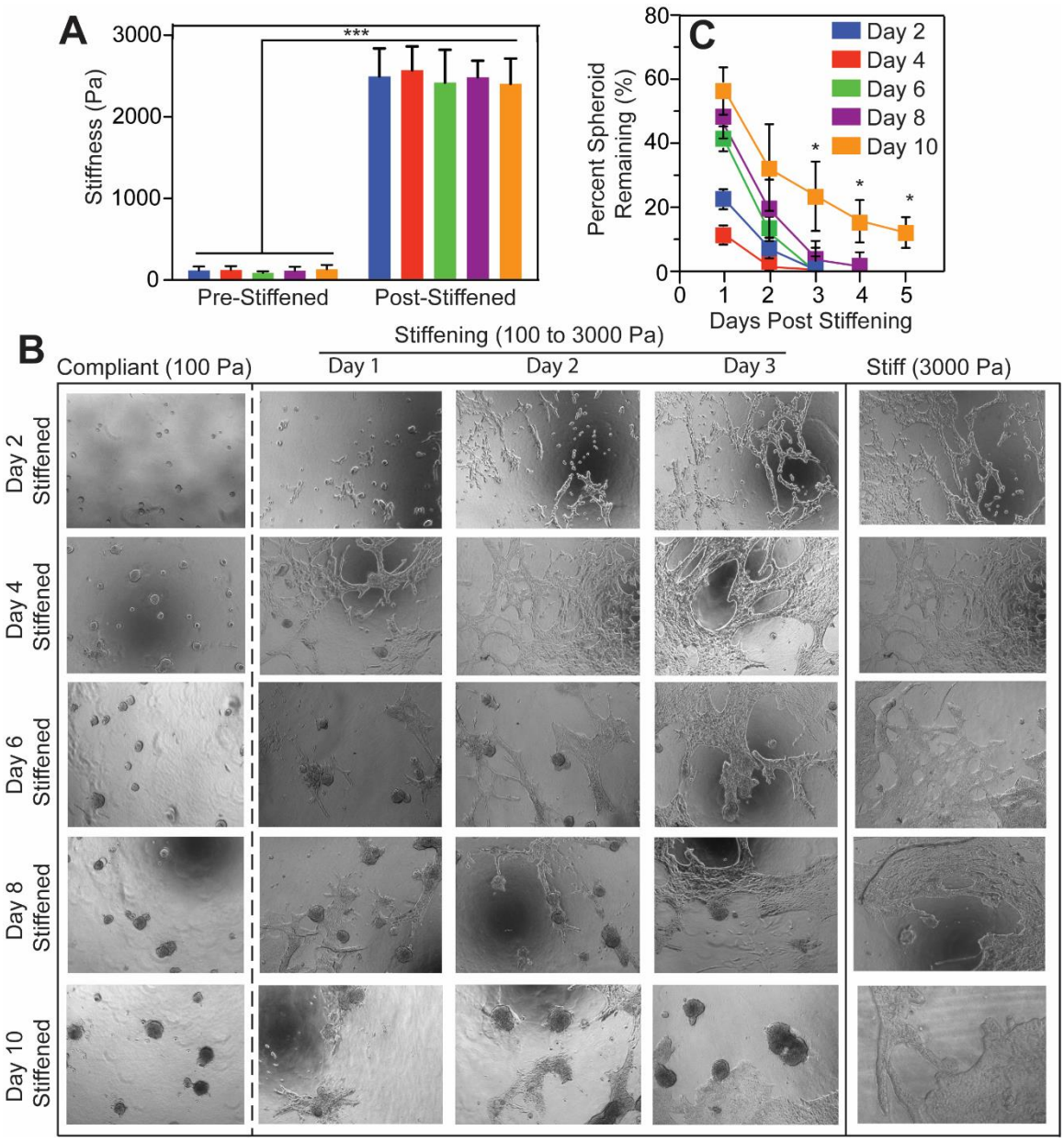

Figure 2.3. Dynamically stiffened MeHA substrates influence MEC stiffness response
(A) On culture days 2, 4, 6, 8, and 10 on 100 Pa substrates, samples were stiffened to approximately 3000 Pa and were similar regardless of the pre-culture period. Data here represent mean ± standard deviation for polymerization from first batch of MeHA (n=6 hydrogels with >100 measurements per bar). ***$p<10^{-3}$ from an unpaired student t-test. (B) Representative brightfield images of MECs cultured on MeHA substrates with variable times for stiffening corresponding to panel A and indicated by row (middle columns); total culture time for dynamically stiffened gels are indicated for each row plus the time indicated by each column. For reference, MECs cultured on substrates with stiffness of 100 Pa (left column) and 3000 Pa (right column) are shown with each row corresponding to the indicated culture day. (C) Quantification of the percent acini remaining as a function of the days post stiffening. Data is sorted by pre-culture time (2-10 days as indicated by color; n= 2 biological replicates with ≥ 2 gels with 80-341 acini measured per condition; for 8 days pre-culture, n= 1 biological replicate with 4 gels with 70-135 acini measured per gel). ****$p<10^{-4}$ for time post stiffening and ***$p<10^{-3}$ for stiffening day from a two-way ANOVA.

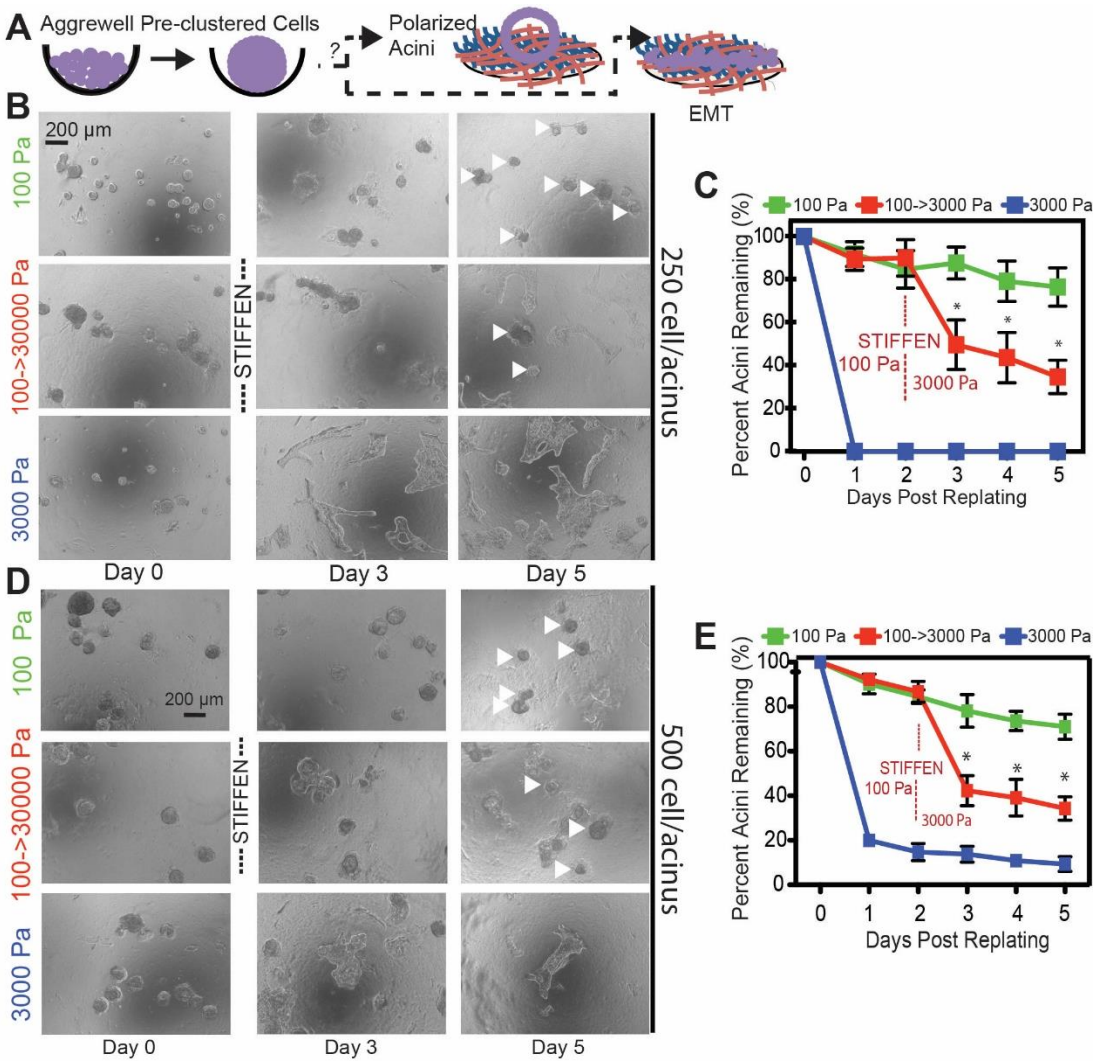

Figure 2.4. Ability of MECs to respond to stiffness-mediated changes is size independent
(A) Schematic shows how aggrewell plates were used to pre-cluster cells prior to seeding onto 100 and 3000 Pa substrates to investigate the dependence on acini size or maturity. (B) and (D) 250 and 500 cells per acinus, respectively, were seeded onto 100 and 3000 Pa substrates, and selected 100 Pa hydrogels were stiffened at day 2. Images show resulting morphology at indicated days. White arrowheads denote the acini remaining on substrates 5 days post-plating. (C) and (E) The percent acini remaining are shown as a function of days post-replating with the day of stiffening indicated for 250 and 500 cells per acinus, respectively. *$p<0.05$ for Tukey's post-hoc analysis versus other conditions (n = 2 biological replicates containing 33-67 acini or EMT cluster/condition/time point).

2.3.3 Stiffening-induced EMT is not a cell autonomous process but is augmented by paracrine signaling

Single MECs have been suggested to have "memory" of their previous niche,[141] and given the heterogeneous responses of acini after stiffening, we next asked if acini

would exhibit memory. Acini were cultured on stiffened hydrogels as in Fig. 3 for 10 days (labeled as 1^o) and remaining acini were separated from spread cells using a differential typsinization method (Supplemental Fig. 4). The separated acini and spread cell populations were then reseeded on soft MeHA substrates that were soft, stiffened, or stiff (labeled as 2^o) to assess whether acini response was cell autonomous (Fig. 5A). When acini were plated onto the secondary hydrogel without stiffening, cells remained acinar, but when plated onto stiff substrates, most acini exhibited EMT-like changes (Fig. 5B-C, green vs. blue). When plated on stiffened 2^o hydrogels, nearly all acini were maintained until stiffening at which point the population became heterogeneous again (Fig. 5B-C, red). Conversely when spread MECs were plated onto stiff 2^o hydrogels, cells remained spread (Fig. 5 D-E, blue), but for both soft and stiffened MeHA, MECs formed acini, which became heterogeneous only when MeHA was stiffened during the 2^o screen (Fig. 5 D-E, green vs. red). To more closely assess phenotype resulting from acini and spread cells in the 2^o hydrogel, we examined E-cadherin localization and found that regardless of input MEC type (acinar or spread), acini on soft MeHA had peripheral E-cadherin localization and typically exhibited hollow centers (Supplementary Fig. 5-6, top). Surprisingly, spread cells on stiff MeHA had similar peripheral E-cadherin localization although they lacked polarized orientation (Supplementary Fig. 5-6, bottom); both results were present when MeHA was stiffened (Supplementary Fig. 5-6, center). Since both cell populations adapted to their local microenvironment and responded when MeHA was stiffened–consistent with the heterogeneous response observed in Fig. 3–these data suggest that cell decisions are not autonomous and rather involve transient and collective signaling among cells within the acinus or cluster of spread MECs.

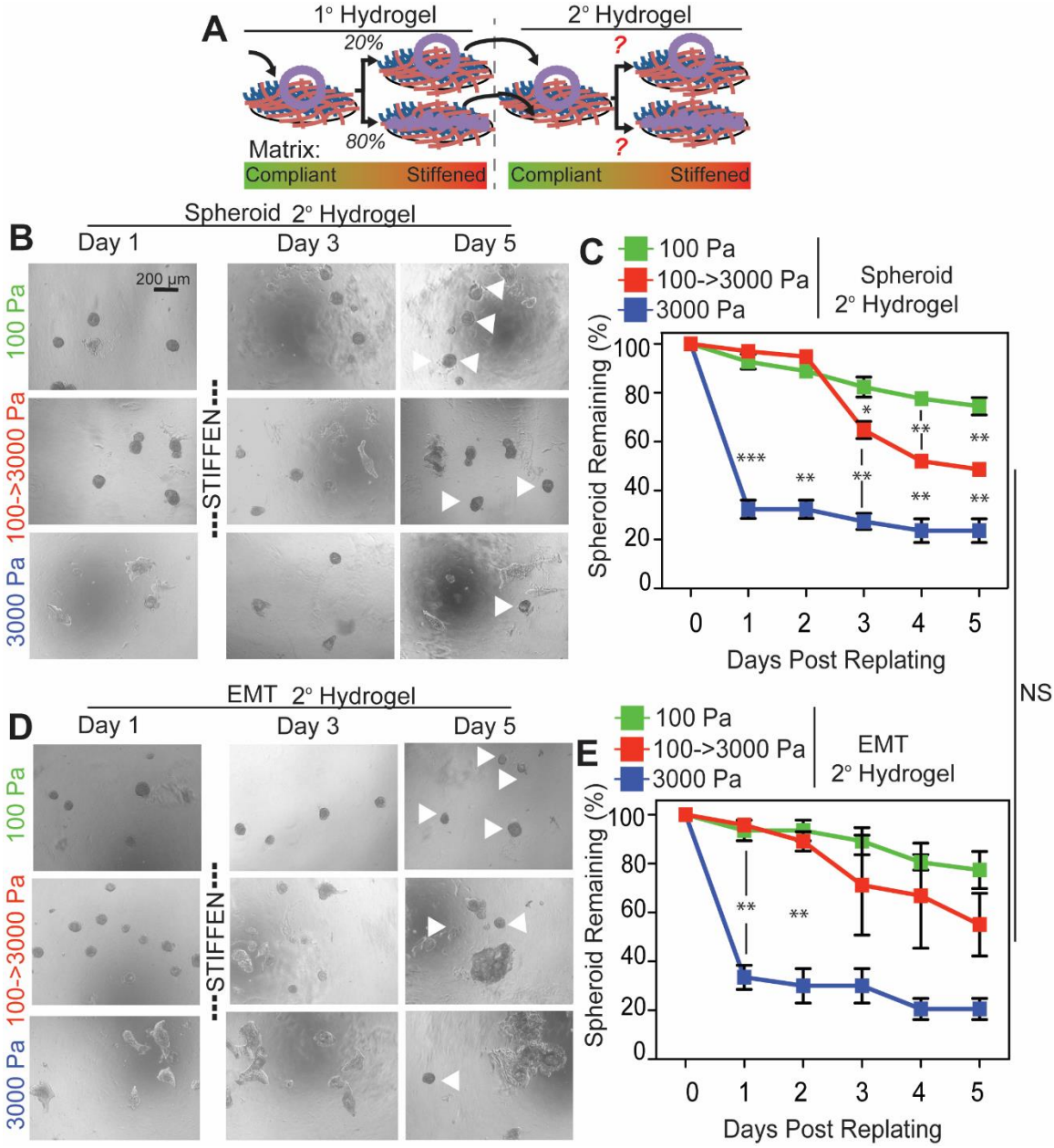

Figure 2.5. MEC spreading is not cell autonomous

(A) Schematic depicting 1° and 2° screens of acini that were cultured on stiffened hydrogels during the 1° screen. Cells undergoing EMT were separated from acini using the method in Supplemental Figure 4 and replated in the 2° screen on 100 Pa, 3000 Pa, or a substrate stiffened from 100 to 3000 Pa. (B) and (D) Representative images up to day 5 post-replating from the 2° screen of cells isolated from acini and EMT regions of the primary screen, respectively. For substrates that were stiffened (middle row), timing of matrix stiffening is noted. White arrowheads denote the acini remaining on substrates 5 days post-plating. (C) and (E) The percent acini remaining are shown as a function of days post-replating with the day of stiffening indicated for cells isolated from acini and EMT regions of the primary screen, respectively (n= 2 biological replicates containing 10-71 acini or EMT cluster/condition/time point). *$p<0.05$, **$p<10^{-2}$, and ***$p<10^{-3}$ for Tukey's post-hoc analysis versus other conditions at the same time point. Two-way ANOVA was not significant for effect of EMT vs. acini.

2.3.4 Heterogeneous stiffening-mediated responses occur via TGFβ and YAP signaling

E-cadherin expression and localization suggests that paracrine signaling may augment collective behavior. TGFβ is a common soluble factor that affects EMT,[35] so exogenous TGFβ was added to culture media of acini from Fig. 5 plated onto soft, stiffened, and stiff substrates to determine to what extent a paracrine signal could influence collective stiffness sensing; in all conditions, the number of acini remaining was greatly reduced, with progressive loss occurring even after stiffening and on soft substrates absent any stiffness signal (Supplemental Fig. 7). Unlike in the absence of TGFβ on stiff MeHA where E-cadherin expression was lower but still localized, we observed complete loss of E-cadherin by day 5 in the presence of TGFβ on stiff MeHA (Supplemental Fig. 8).

Given that exogenous TGFβ induced increased spreading on all conditions but especially on stiffened MeHA, we next assessed stiffness-mediated localization of SMAD2/3, a signaling complex immediately downstream of TGFβ receptor, and Twist, a basic helix loop helix transcription factor associated with stiffness mediated EMT.[101,142] Both SMAD and Twist nuclear localized on pathologically stiff (Fig. 6A, solid arrowheads) but not physiologically soft matrices (hollow arrowheads) (Fig. 6A-B). For stiffened hydrogels, both acinar and spread cell subpopulations exhibited heterogeneous distributions of localized (solid arrowheads) and non-localized (hollow arrowheads) SMAD and Twist (Fig. 6C-D). Additionally when cells on stiff and stiffened conditions nuclear localized SMAD, we observed its phosphorylation (Supplemental Fig. 9), indicating a transcriptionally active and stiffness responsive SMAD complex. To decouple TGFβ signaling from stiffening-induced responses, 10 μM Galunisertib, a TGFβ receptor

inhibitor, was added to culture media of acini on soft substrates that were subsequently stiffened. Although inhibition prevented SMAD2/3 nuclear localization and also subsequent localization changes for Twist (Supplemental Fig. 10A-B), a subset of cells still left acini, spread, and became motile (Supplemental Fig. 10C). However, this population was significantly smaller and less migratory in Galunisertib-treated acini (Supplemental Fig. 10D-E). These data suggest that stiffening on MeHA substrates induces a collective paracrine cell response via TGFβ signaling which in turn activates canonical EMT pathways in many spreading cells, but there remains a fraction of acini whose collective response appears independent of TGFβ and Twist.

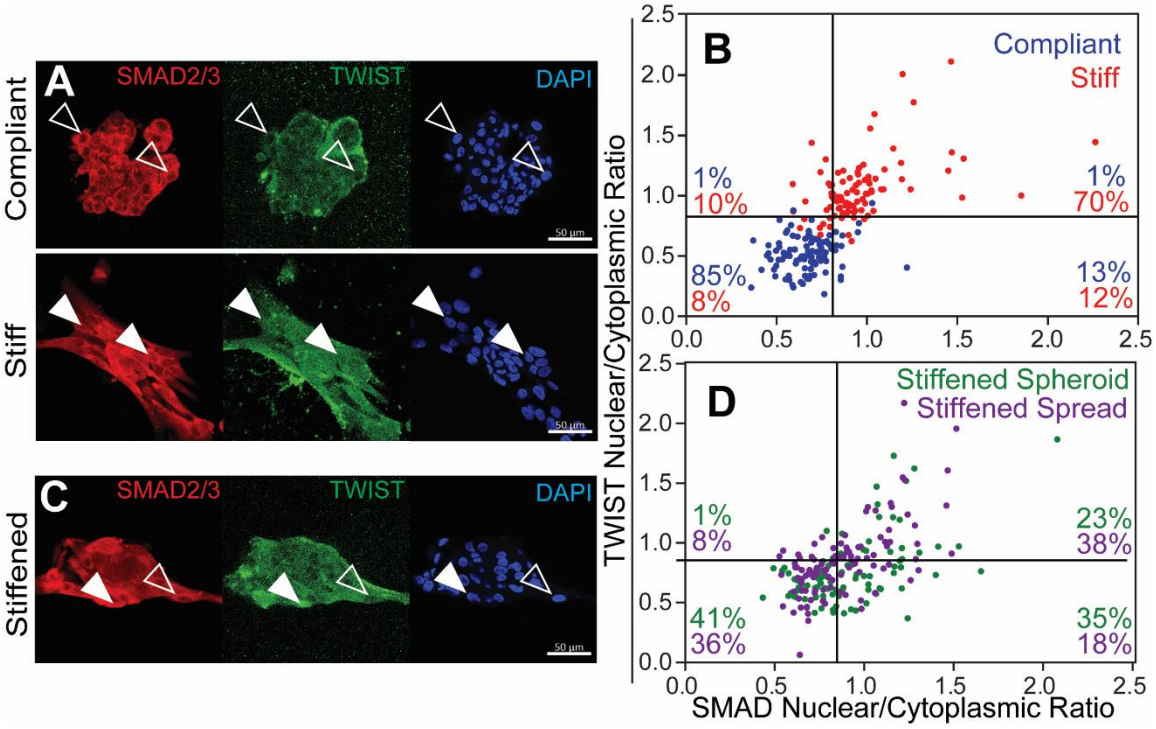

Figure 2.6. TWIST and SMAD localization in acinar and spread MECs
(A) TWIST (green) and SMAD2/3 (red) immunofluorescent imaging of MECs on soft and stiff MeHA substrates. Images show cells that have cytoplasmic localization of TWIST and SMAD (hollow arrowheads) on soft gels and nuclear localization (filled arrowheads) on stiff gels. (B) Plot of the nuclear to cytoplasmic intensity ratio for Twist and SMAD2/3 for the indicated conditions (n=100 cells). Lines delineate separation of data between soft and spread cells. (C) TWIST and SMAD2/3 immunofluorescent imaging for MECs on stiffened MeHA substrates. Arrowheads indicate cells that are cytoplasmic or nuclear localized. (D) Plot of the nuclear to cytoplasmic intensity ratio for Twist and SMAD on stiffened substrates (n=100 cells). The delineated lines from Panel B were used to identify cells as either positive or negative for the markers.

To determine the underlying mechanism for non-SMAD/Twist spread cells when exposed to dynamic matrix stiffness, we assessed the localization and activity of the mechanosensitive transcription activator Yes-associated protein 1 (YAP)[94, 95] which has been recently implicated in several metastatic cascades.[91, 96] As with Twist, YAP nuclear localization was observed on stiff hydrogels but not soft (Fig. 7A, bottom). However on stiffened hydrogels, 29% of cells had nuclear localized YAP but not SMAD (Fig. 7C-D); conversely only 8% of cells were Twist but not SMAD2/3 positive (Fig. 6D). Furthermore, TGFβ receptor inhibition resulted in clear stratification of the acinar and spread, motile subpopulations into YAP non-localized and YAP localized groups, respectively (Supplemental Fig. 11A-B), suggesting a role for YAP in initiating non-TGFβ-mediated spreading. To understand the role of YAP activity in the spread cell phenotype, we inhibited its activity with Verteporfin, a small molecule that reduces endogenous YAP expression and prevents nuclear activation.[148] While Verteporfin reduced YAP nuclear expression, it did not inhibit spreading on stiff hydrogels (Supplemental Fig. 12). Interestingly, YAP inhibition on stiffened gels resulted in a significant reduction of spreading and migration similar to TGFβ receptor inhibition (Supplemental Fig. 13). However while YAP or TGFβ receptor inhibition alone resulted in significantly fewer spread and motile cells per acini, dual inhibition provided the greatest overall reduction in the total number of spread, motile cells (Fig. 8A-B). Together these data suggest that collective signaling throughout the acinus may be sensed through a combination of both paracrine signaling via TGF-β/SMAD and mechanical signaling via YAP localization, and that when jointly inhibited, acini composed of MECs give rise to significantly fewer cells capable of spreading and migrating into the surrounding stroma (Fig. 8C).

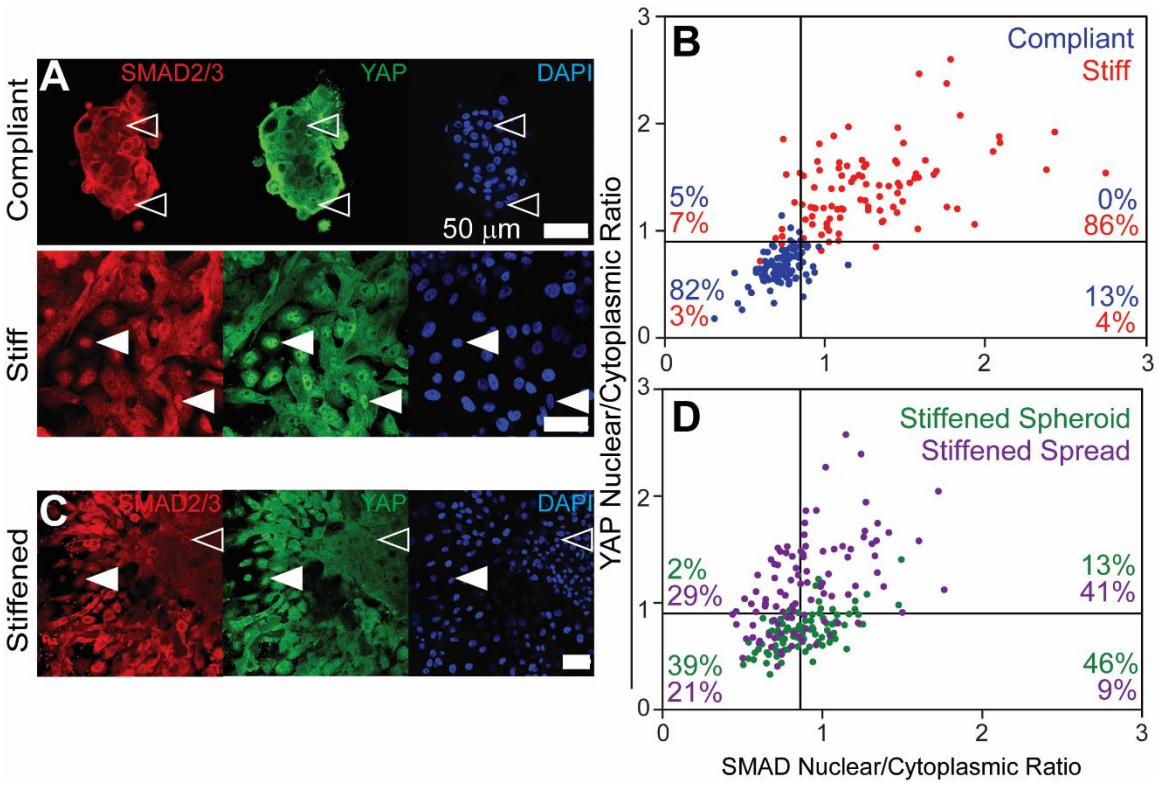

Figure 2.7. YAP and SMAD localization in acinar and spread MECs
(A) YAP (green) and SMAD2/3 (red) immunofluorescent imaging of MECs on soft and stiff MeHA substrates. Images show cells that have cytoplasmic localization of YAP and SMAD2/3 (hollow arrowheads) on soft gels and nuclear localization (filled arrowheads) on stiff gels. (B) Plot of the nuclear to cytoplasmic intensity ratio for YAP and SMAD2/3 for the indicated conditions (n=100 cells). Lines delineate separation of data between soft and spread cells. (C) YAP and SMAD2/3 immunofluorescent imaging for MECs on stiffened MeHA substrates. Arrowheads indicate cells that are cytoplasmic or nuclear localized. (D) Plot of the nuclear to cytoplasmic intensity ratio for YAP and SMAD2/3 on stiffened substrates (n=100 cells). The delineated lines from Panel B were used to identify cells as either positive or negative for the markers.

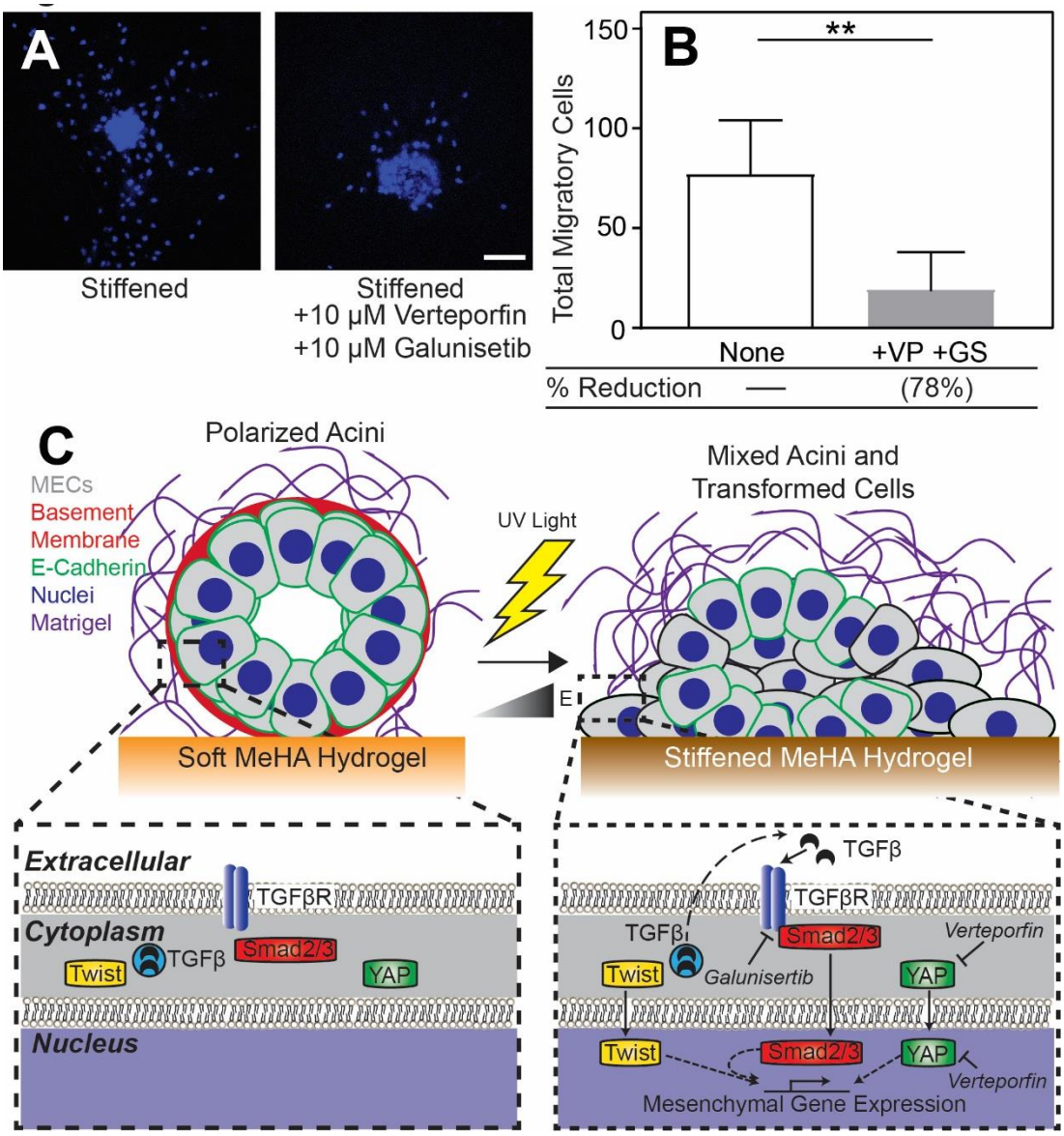

Figure 2.8. YAP and SMAD inhibition reduces number of spread cells in MECs on stiffened gels
(A) Representative image demonstrating spread cells on stiffened substrates and cells treated with Galunisertib and Verteporfin. (B) Total number of spread cells per acinus were plotted for untreated and treated cells. *$p<0.05$, **$p<10^{-2}$, and ***$p<10^{-3}$ for Tukey's post-hoc analysis. (C) Mechanism describing inhibition of YAP and SMAD nuclear localization on MECs spreading.

2.4 Conclusion

MeHA-based hydrogels recapitulate mammary morphogenesis *in vitro* as classic, static biomaterial systems do,[101,134] but its ability to be dynamically stiffened to mimic *in vivo* pathogenesis provides a new tool to elucidate events and signaling not otherwise

observable under static conditions, e.g. dual TGF-β/SMAD and YAP collective signaling versus that previously observed with Twist and integrins. Here, we show that pre-culture on soft substrates resulted in a population of acini that were partially resistant to stiffness-mediated spreading. MEC response depended on not only the magnitude of dynamic stiffening, but also the timing of substrate stiffening. We also demonstrated that the MECs did not exhibit "memory"-like behavior but rather that stiffness-dependent MEC responses at the local cell level were modulated by TGFβ and YAP signaling; augmenting or inhibiting this signal induced collective EMT or caused stiffness-sensitive cells to respond and migrate individually, respectively. These results implicate a more complex interplay of paracrine and time-dependent stiffness-mediated cellular changes leading to EMT than suggested by previous static models[14, 62] but in line with *in vivo* systems.[125,132,149] Similar complexities have been observed in other contexts and suggest that broader biomaterials exploration is required; for example, mechanical signaling dynamically changes in conjunction with matrix remodeling. Caliari and colleagues demonstrated that dynamic stiffening provided insight into how pre-culture on soft substrates decreases the time required for YAP translocation post stiffening.[86] Dynamic stiffening also can control cell fate, e.g. cardiomyocyte differentiation, by turning on and off mechanically sensitive pathways over time.[97] Beyond stiffness alone, this phenomenon of dynamic biomaterial properties regulating cell fate–from stem cells to cancer–may extend to topography,[98] surface adhesion,[99] and porosity,[100] and thus warrants increasing attention from the biomedical engineering community.

2.5 Methods

2.5.1 Methacrylated hyaluronic acid (MeHA) polymer synthesis

MeHA was synthesized as previously described.[143] 50 kDa sodium hyaluronate (Lifecore Biomedical, cat # HA40K) was dissolved in de-ionized water at 1 w/v% overnight and reacted with methacrylate anhydride (Sigma-Aldrich, cat # 276685, 6 mL of methacrylate anhydride for 1 g of sodium hyaluronate) at pH 8, followed by overnight incubation, and further reacted with methacrylate anhydride (3 mL of methacrylate anhydride for 1 g of sodium hyaluronate) at pH 8 for 4 hours. MeHA was precipitated out of solution by mixing ethanol with the solution at a ratio of 9:1. After centrifugation, the excess solution was removed and MeHA was dissolved in deionized water followed by dialysis (Spectrum Labs, cat # 132655) against de-ionized water at 4 C for 3 days. Samples were then placed in a lyophilizer (Labconco FreeZone2.5) for another 3 days. The lyophilized MeHA was analyzed by ^{1}H magnetic resonance (NMR) to determine methacrylate substitution ratio by normalization of the peaks at a chemical shift of 6 ppm, representing the methacrylate group, by peaks between 3 and 4 ppm, which represent native HA. Substitution ratios were computed from triplicate NMR analyses (Supplemental Figure 1A). The degree of modification varied by batch but always fell within 35-50% substitution ratio.

2.5.2 MeHA and polyacrylamide hydrogel formulation

MeHA hydrogels were cast onto 12 mm glass coverslips. Coverslips were cleaned via sonication in 70% EtOH for 10 min followed by a secondary sonication in DI H2O for 10 min. After cleaning, coverslips were dried and treated with 0.1 mg/mL poly-d-lysine (Sigma-Aldrich, 70-150 kDa, P6407) for 5 min at room temperature. The poly-d-lysine

was then aspirated and the coverslip rinsed 1x with DI H2O and allowed to dry for at least 2 hours prior to casting gel on the surface.

1% w/v MeHA was dissolved in 0.2 M Triethanolamine (Sigma-Aldrich, cat # T58300) and phosphate-buffered saline (PBS) solution. Irgacure 2959 (Sigma-Aldrich, cat # 410896) was initially dissolved at 1% w/v in ethanol and then diluted to 0.01% w/v in the MeHA solution. 15 μL of the hydrogel solution was sandwiched between a 12 mm poly-d-lysine treated glass coverslip to permit hydrogel binding and a nonadherent dichlorodimethylsilane (Acros Organics, cat # AC11331)-activated glass slide to achieve easy detachment and photopolymerized using a transilluminator (4 mW/cm^2, UVP) emitting 350 nm wavelength UV light. Initial polymerization to create a hydrogel of approximately 100-200 Pascal required ~100 seconds of UV exposure. Subsequent polymerization to stiffen the hydrogel depended on exposure time but ranged from 90 to 150 seconds, depending on the desired final modulus using 1% w/v Irgacure and the degree of methacrylation as measured by NMR.[92] Protein for cell attachment was added by mixing 20 mM 1-ethyl-3-(3-dimethylaminopropyl) carbodiimide (ProteoChem, cat # c1100), 50 mM N-hydroxysuccinimide (Alfa Aesar, cat #A10312), and 150 μg/mL type I rat tail collagen (Corning, cat # 354236) dissolved in PBS. The collagen-crosslinker solution was added to the hydrogel and incubated overnight at 37 C.

For experiments involving PA hydrogels, 12 mm glass coverslips were methacrylated by first oxidizing the surface via UV/ozone exposure (BioForce Nanosciences) followed by functionalization with 20 mM 3-(trimethoxysilyl)propyl methacrylate (Sigma-Aldrich, cat # 440159) in ethanol. A polymer solution containing either 3%/0.03% acrylamide/bis-acrylamide (Fisher) for soft hydrogels or 5%/0.15% for

stiff hydrogels, 1% v/v of 10% ammonium persulfate (Fisher), and 0.1% v/v of N,N,N',N'-Tetramethylethylenediamine (VWR) was prepared. 15 μL of hydrogel solution was sandwiched between a functionalized coverslip and a dichlorodimethylsilane-treated glass slide and polymerized for 15 minutes. Hydrogels were incubated in 0.2 mg/ml sulfo-SANPAH (Fisher, cat # 22589) in sterile 50 mM HEPES pH 8.5, activated with UV light (wavelength 350 nm, intensity 4 mW/cm^2) for 10 minutes, washed three times in HEPES, and then incubated in 150 μg/mL collagen solution (Corning) overnight at 37ºC.

2.5.3 Atomic force microscopy and force spectroscopy

Hydrogel stiffness measurements were determined by atomic force microscopy (MFP-3D Bio, Asylum Research) with a silicon nitride cantilever (NanoAndMore USA Corporation, cat # PNP-TR). Tip deflections were converted to indentation force for all samples using their respective tip spring constants and Hooke's Law. All AFM data was analyzed using custom-written code in Igor Pro (Wavemetrics) to determine Young's Modulus as previously described based on a Hertz model.[154] Note that code is available at http://ecm.ucsd.edu/AFM.html and simply requires MATLAB to run. Conversely, protein tethering quantification by force spectroscopy was analyzed as previously described.[93] Cantilevers were functionalized with an anti-collagen type I antibody (Sigma, cat # C2456), or avidin (Prospec, cat # PRO-500) using a previously established method. Briefly, cantilevers were cleaned with chloroform and immersed in ethanolamine-HCl in dimethyl sulfoxide. Tips were incubated in bis(sulphosuccinimidyl)suberate (Fisher, cat # 21580), rinsed, and then immersed either in an antibody or avidin solution to crosslink the protein to the tip. Force curves were taken in a regular 10 × 10 array of points spaced ~10 μm apart. To promote binding of the antibody to collagen or avidin

to biotin, a dwell time of 1 s was added between approach and retraction cycles. Force curves were converted to force versus tip position. *Z*-position curves and then analyzed for rupture events using a previously described algorithm; rupture events were then determined.

2.5.4 Cell culture

MCF10A cells were cultured as previously described.[127] Briefly, cells were maintained in growth media containing DMEM/F12 (Gibco, cat # 11320) with 5% Horse serum (Omega Scientific, cat # DH-05), 20 ng/mL hEGF (Peprotech, cat # AF-100-15), 0.5 μg/mL hydrocortisone (Sigma, cat # H0888), 100 ng/mL Cholera toxin (List Biological Laboratories, cat # 100B), 10 μg/mL insulin, and 10 U/mL Pen/Strep (Gemini Bio-Products, cat #400-109). Upon reaching about 80% confluency, cells were treated with 0.05% trypsin (Gibco, cat # 25300054) for 5 minutes to dissociate cells. Trypsin was neutralized with DMEM/F12 with 20% horse serum and 10 U/mL pen/strep and replated in growth media for future cultures.

For hydrogel experiments, cells were cultured in assay media containing DMEM/F12 with 2% Horse serum, 5 ng/mL hEGF, 0.5 μg/mL hydrocortisone, 100 ng/mL Cholera toxin, 10 μg/mL insulin, and 10 U/mL Pen/Strep. After trypsinization, cells were resuspended in a combination of assay media and 2% Matrigel (Corning, cat # 354277) for seeding onto collagen functionalized HA gels directly at 3000 cells/well. Media was exchanged every 4 days. To preform spheroids, MCF10As were added to rinsed Aggrewell 400 plates (Stem Cell Technologies, cat # 34411) and seeded at 50-500 cells per spheroid as per the manufacturer's directions using 0.25% Methocult (Stem Cell Technologies, cat # H4434). The spheroids were then cultured in assay media prior to resuspension and

seeding using 2% Matrigel onto functionalized HA hydrogels. After preculture, hydrogels were incubated in media plus 0.5 mg/mL Irgacure 2959 for 30 minutes at 37^{o}C. The hydrogels were then stiffened using UV light (350 nm) exposure for approximately 2 minutes. All controls and unstiffened samples were treated with the same UV exposure. Post-stiffening hydrogels were rinsed with 1x media volume of PBS and then placed back into assay media. Cell apoptosis was probed using a p53 antibody (Thermo, cat # AHO0152, 1:250). For experiments investigating the addition of TGF-β, TGF-β was first dissolved in 10 mM acetic acid before addition to assay media at a concentration of 5 ng/mL. To determine cell adhesion to hydrogel surface, cells were seeded onto the surface of hydrogels and given 30 minutes to adhere. After 30 minutes, cells were washed three times and the number of cells remaining was counted.

Galunisertib (Selleckchem, cat # S2230) was stored at -80°C and Verteporfin (Cayman Chemical, cat # 17334) was stored at -20°C suspended at 10 mM and 50 mg/mL respectively in dimethylsulfoxide (Sigma, cat #D2650). For experiments inhibiting TGFβ or YAP, Galunisertib or Vertiporfin was added to sample assay media to produce a final concentration of 10 μM. Galunisertib was added immediately following seeding for soft or stiff samples and was added prior to stiffening for the stiffened samples to the assay media and was maintained post stiffening. Verteporfin was added immediately following seeding (for soft or stiff samples) or immediately following stiffening (for stiffened samples).

2.5.5 Primary and secondary screening assay

MCF10A cells were seeded at $10^4/cm^2$ onto protein-coated MeHA hydrogels prior to overlay as described above for data in Figures 1-3 and Supplemental Figures 1-4. Hydrogels were dynamically stiffened on days 2, 4, 6, 8, and 10 post seeding. Unseeded

control hydrogels were tested concurrently with the AFM to determine their Young's modulus to ensure repeatable stiffening. Cell morphology was characterized by determining the percent acini remaining post stiffening up to 5 days after the stiffening event. For Figures 4-6 and Supplemental Figures 5-9, soft and stiff MeHA hydrogels were seeded with a MCF10A preformed spheroids at approximately 250 or 500 cells per spheroid as indicated or, if not, at 250 cells per spheroid. After two days of culture, a subset of the soft hydrogels was subjected to stiffening. All samples with and without Irgacure were subjected to the same UV exposure. Post stiffening, the hydrogels were rinsed with 1x PBS and placed back into assay media. Morphology of the cells was observed daily and percent acini remaining was determined up until day 5.

Acini were separated from spread cells using an EDTA rinse to remove for replating onto soft or stiff substrates to perform a secondary screen. The spread cells were removed using trypsin and seeded onto soft and stiff substrates for an additional secondary screen. In all cases, the cells were cultured on the substrates for 2 days prior to the stiffening event and the percent remaining acini was determined.

2.5.6 Immunostaining and analysis

Hydrogels were rinsed with PBS containing 250 mM $MgCl_2$ (Solution A) and fixed using 3.7% formaldehyde in Solution A for 15 minutes at RT. Samples were then rinsed 2x with Solution A. Matrigel was removed by adding PBS with 5 mM EDTA (Fisher, cat # BP20-1) to the hydrogels and incubated at 4C for 30 minutes. Samples were then rinsed with cold PBS and permeabilized using 0.5% Triton-X 100 for 15 minutes at RT. Blocking was carried out in a 20% goat serum + 0.2% Triton-X 100 in PBS solution for 30 minutes at RT. Primary antibodies were then incubated overnight at 4C with the following dilutions:

Anti-laminin (abcam, ab11575, 1:100); E-cadherin (BD, 610181, 1:50); pSMAD2/3 (Cell Signaling Technology, D27F4, 1:100); SMAD2/3 (Cell Signaling Technology, D7G7, 1:1600); TWIST (Santa Cruz Biotechnology, sc-81417, lot: J2213, 1:25); YAP (Santa Cruz Biotechnology, sc-101199, 1:50). Samples were rinsed 3x with PBS for 5 min and incubated with secondary antibodies (Goat anti-mouse 488 (Invitrogen, A11004, lot 1218263)/ Goat anti-rabbit 568 (A11011, Lot 1345045)) for 1 hour in 20% goat serum + 0.2% Triton-X 100 in PBS at RT. Samples were rinsed 3x with PBS for 5 min and nuclei were counterstained using Hoechst 33342 (Invitrogen, H3570, 1:7500) or DAPI for 15 min at RT in PBS. They were then rinsed 3x with water and mounted onto glass slides using Fluoromount-G (Southern Biotech, cat # 0100-01). After waiting 1 hour, mounted samples were sealed using clear nail polish. Samples were kept at 4C until imaging on a Zeiss LSM 780 confocal using a 40x water immersion objective. For IF images shown, z-stacks were acquired and max intensity projections were made using ImageJ unless otherwise noted in the figure legend. No non-linear modifications were made to acquired images utilized for analysis.

Individual cells were analyzed for SMAD2/3, TWIST, and/or YAP nuclear localization using ImageJ. In addition to DAPI, samples were counterstained for combinations of SMAD and TWIST or SMAD and YAP as described above. DAPI staining was used to identify the cell's nuclear region which was measured for the average fluorescent intensity of the protein of interest. Measurements were then normalized to the cell's average cytoplasmic fluorescent intensity producing the nuclear to cytoplasmic ratio presented. Spreading and proliferation were also assessed using ImageJ. Bright field images were used to determine the central acinus' margins for individual cell colonies. This

region was then superimposed on identical DAPI stained images which were converted to a binary mask. Particles outside the margins were identified as spreading cells and were counted and measured for X and Y positions to produce a number of spreading cells and migratory distance per colony.

2.5.7 Statistical analysis

Statistical significance was determined using an ANOVA with Tukey's post-hoc analysis unless otherwise denoted, with the threshold for significance level set at $p<0.05$. Means are reported ± standard deviation for all experiments.

2.6 Supplementary Figures

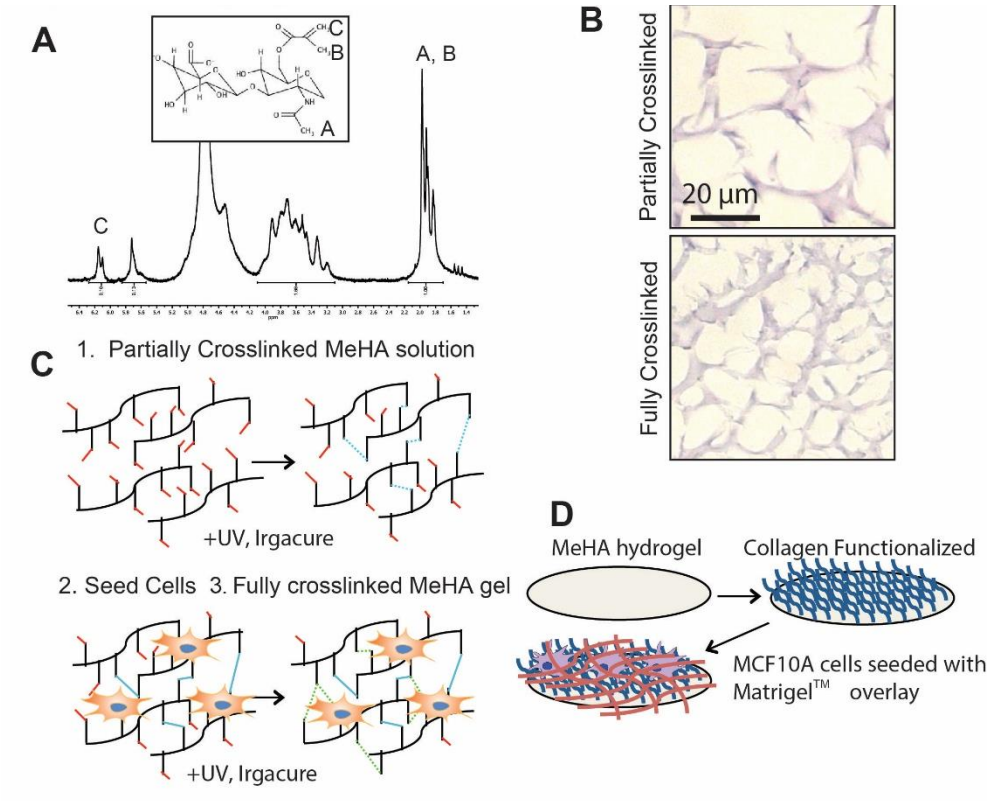

Supplementary Figure 2.1. Characterization, polymerization, and cell seeding onto methacrylated hyaluronic acid (MeHA) hydrogels. (A) NMR spectra of synthesized methacrylated HA with inset image of the HA backbone with letters indicating which peaks correspond to regions of the molecule. (B) Images of cryosectioned MeHA hydrogels having undergone one (partially) or two (fully) cycles of crosslinking. (C) Schematic of MEC seeding onto the hydrogels relative to the two-stage crosslinking processes. (D) Illustration of how the partially crosslinked MeHA is functionalized with collagen and cells are seeded in Matrigel overlay before becoming fully crosslinked.

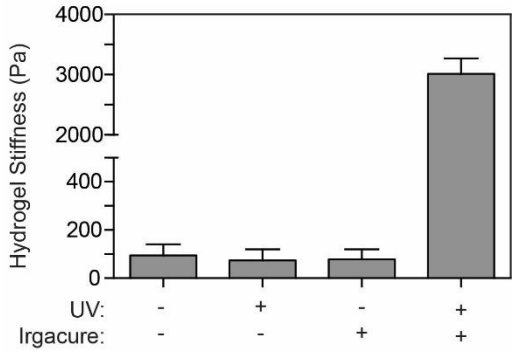

Supplementary Figure 2.2. Stiffening is dependent on the presence of both a free radical donor and UV light
Plot displays MeHA hydrogel stiffness, as measured by AFM, for the combinations of Irgacure initiator and UV shown (n = 5 or more hydrogels with >20 measurements per gel/bar).

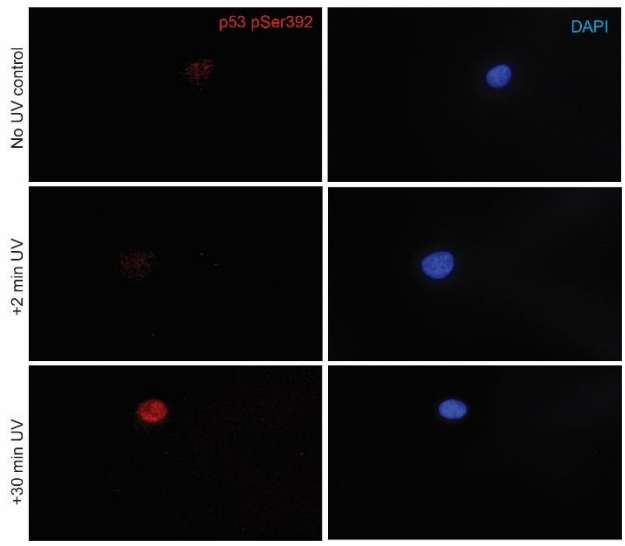

Supplementary Figure 2.3. Stiffening does not induce DNA damage
MECs were exposed to UV radiation for the indicated time and resulting images of p53 activation, which is indicated by phosphorylation at Ser392 (red), are shown.

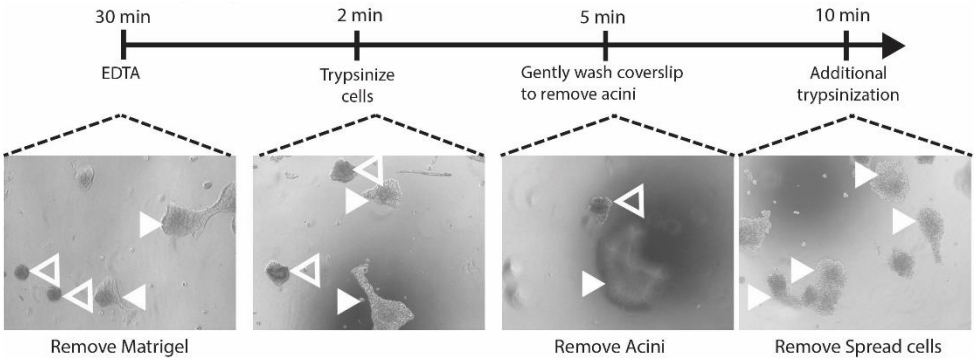

Supplementary Figure 2.4. Separation of acini and spread cells from MEC cultures
Images and the timeline highlight the differential typsinization steps required to separate acini (open arrows) from spread cells (close arrows). Substrates first have their Matrigel overlay removed by EDTA, then acini are removed using trypsin and a gentle wash, and finally the spread cells are removed by an additional, longer trypsin incubation.

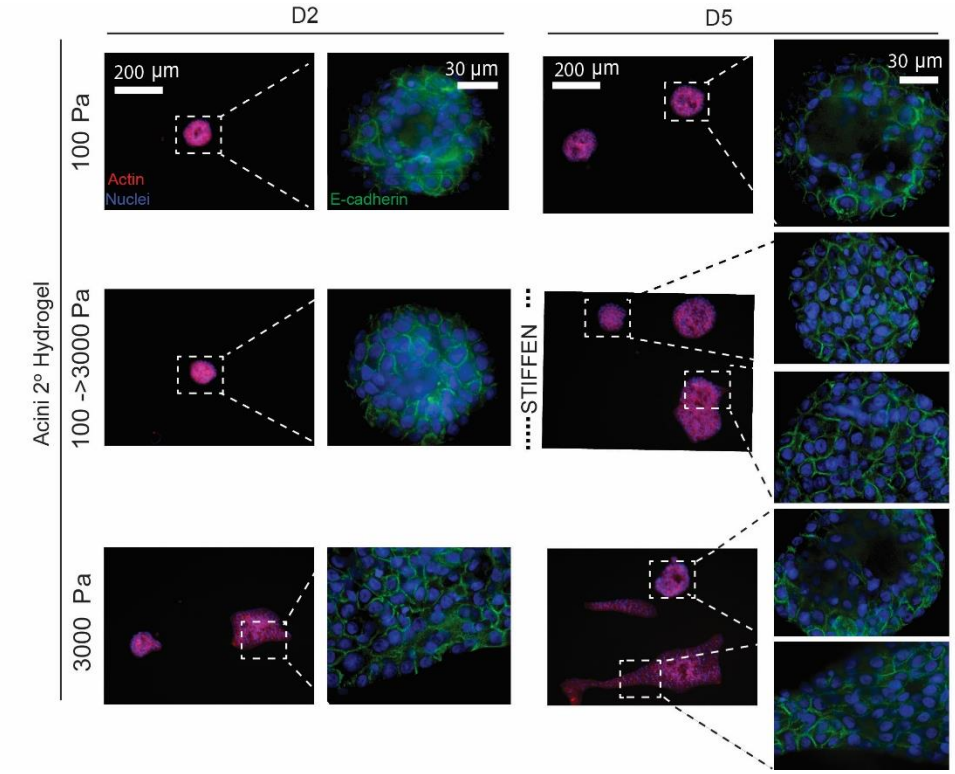

Supplementary Figure 2.5. E-Cadherin junctions and spreading do not exhibit memory from acinar culture
MECs that remained in acinar structures post-stiffening and were re-plated onto 100 Pa, 3000 Pa, and substrates stiffened from 100 to 3000 Pa were imaged for actin (red), E-cadherin (green), and nuclei (blue). Images are show at days 2 and 5 and represent both spread and acinar morphologies depending on the niche. Scale bar is 200 and 30 µm for low and high magnification images, respectively.

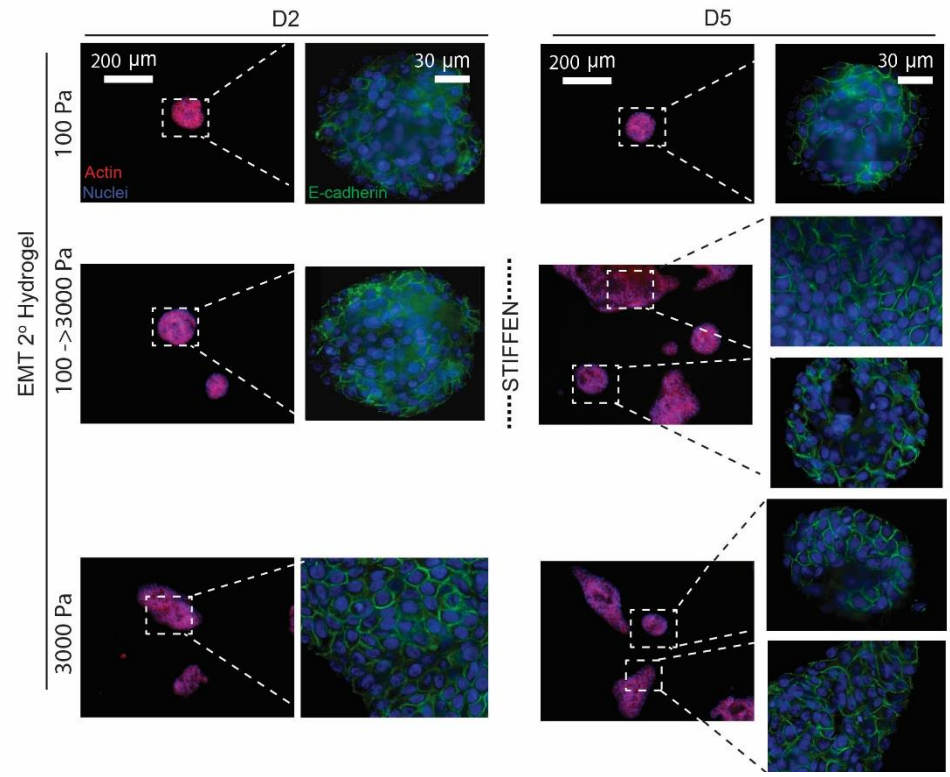

Supplementary Figure 2.6. E-Cadherin junctions and spreading do not exhibit memory from EMT culture MECs that spread post-stiffening were re-plated onto 100 Pa, 3000 Pa, and substrates stiffened from 100 to 3000 Pa were imaged for actin (red), E-cadherin (green), and nuclei (blue). Images are show at days 2 and 5 and represent both spread and acinar morphologies depending on the niche. Scale bar is 200 and 30 µm for low and high magnification images, respectively.

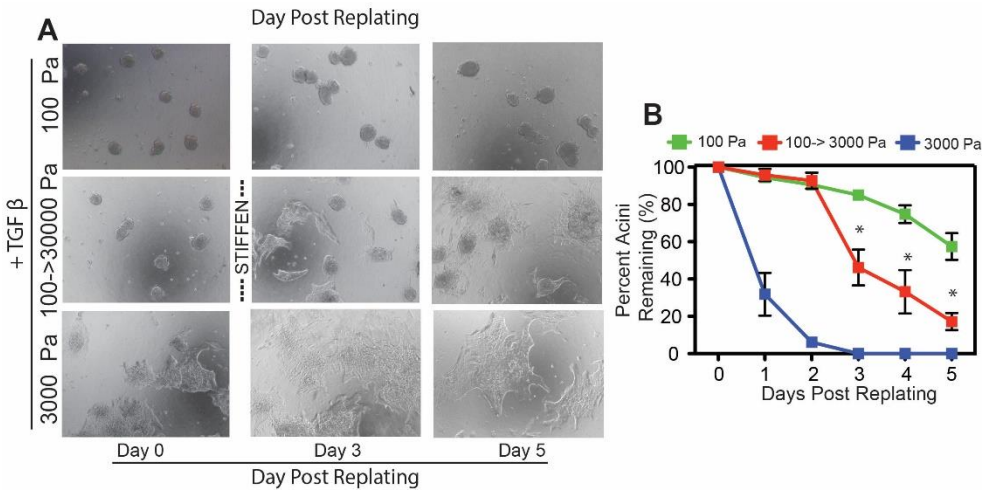

Supplementary Figure 2.7. Exogenous TGF-β reduces remaining acini
(A) Brightfield images show MCF10A acini plated onto 100 Pa and 3000 Pa hydrogels as well as 100 Pa substrates that were stiffened to 3000 Pa at day 2 post-TGF-β addition and re-plating. (B) Plot shows quantification of the percent acini remaining as a function of time on the hydrogel (n >2 biological replicates containing 50 acini/condition). *p <0.05 by two-way ANOVA with Tukey's post-hoc analysis.

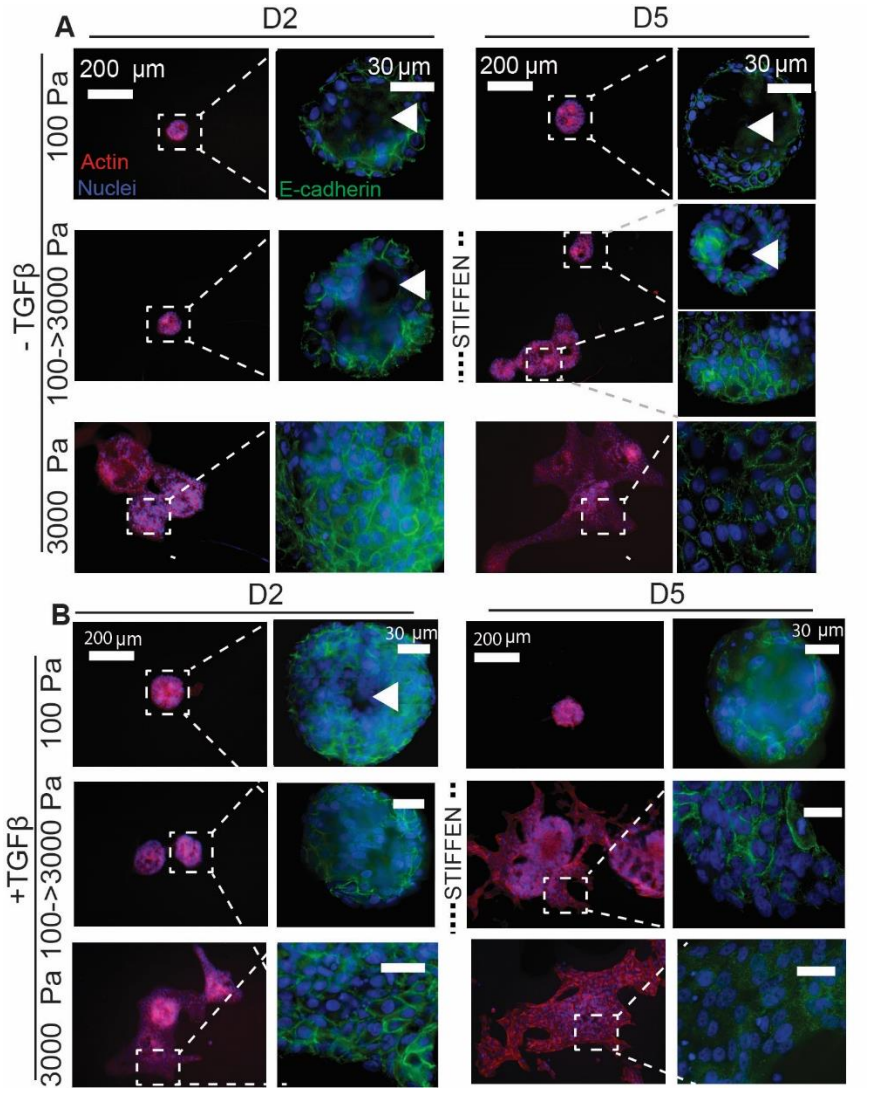

Supplementary Figure 2.8. Exogenous TGF-β influences E-cadherin expression
Immunofluorescent images of MCF10A cells, preclustered via aggrewells and then cultured on the indicated MeHA hydrogels (A) in the absence or (B) presence of exogenously added TGF-β for the indicated number of days. Low magnification images show actin staining (red) whereas higher magnification images show E-cadherin localization (green); nuclei are stained with DAPI (blue). Dynamic stiffening occurred for hydrogels in the middle rows at the indicated time point. Arrowheads indicate regions that have begun to hallow. Scale bar is 200 and 30 µm for low and high magnification images, respectively.

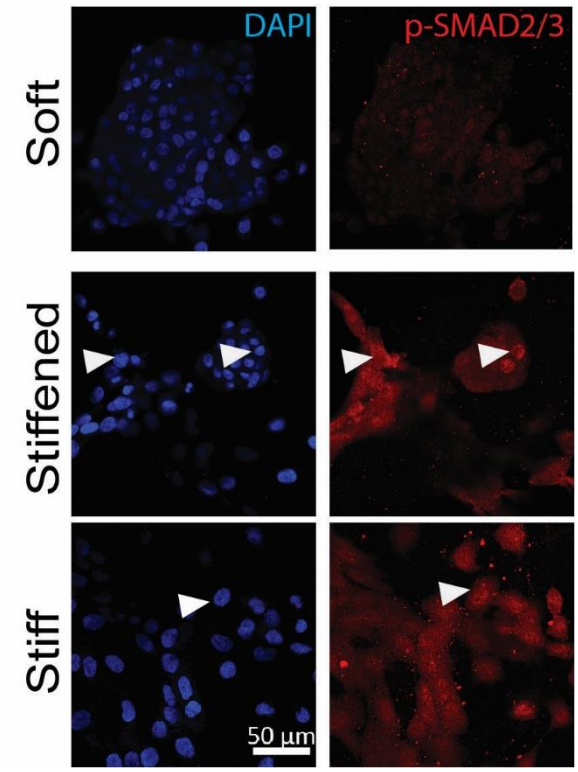

Supplementary Figure 2.9. SMAD phosphorylation in MECs on stiffened or stiff substrates. Immunofluorescent images of p-SMAD (red) and nuclei (blue). Arrowheads indicate cells that are positive for SMAD phosphorylation. Scale bar is 50 μm.

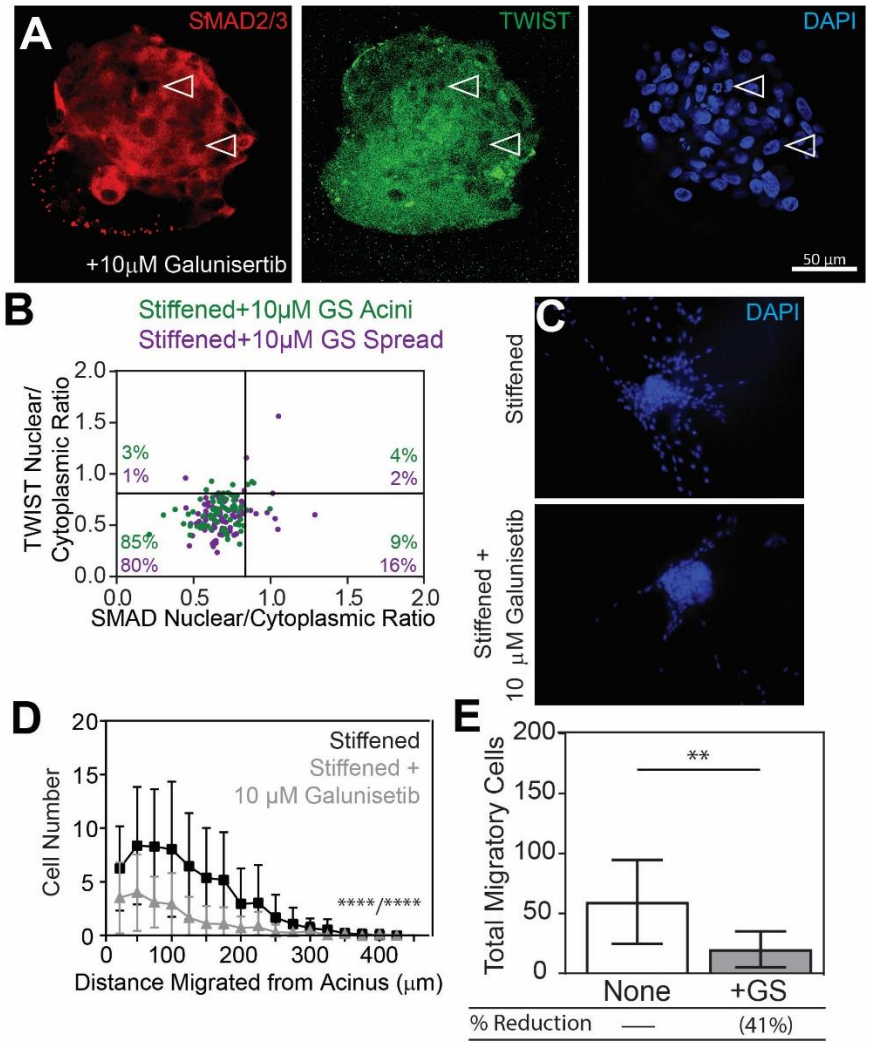

Supplementary Figure 2.10. TGF-β inhibition via galunisertib reduces MCF10A spreading on stiffened hydrogels. (A) Immunofluorescent images of SMAD2/3 (red) and TWIST (green) in MCF10A cells grown on stiffened hydrogels and treated with Galunisertib. Hollow arrowheads indicate cells that are negative for markers. (B) Plot of the nuclear to cytoplasmic intensity ratio for Twist and SMAD (n=100 cells). Delineated lines indicate cells that are positive or negative for the markers based on controls in Figure 6B. (C) Fluorescent images of cells on stiffened substrates selectively treated with 10 μM Galunisertib and stained with Hoechst (blue). Scale bar is 100 μm. (D) Histogram plot of distance traveled from the acinus for cells in drug treated (grey) and non-treated (black) groups. ****p $<10^{-4}$ by two-way ANOVA for both distance and drug treatment (n = 12 acini/condition/experiment from duplicate assessments). (E) The total number of cells migrating out of MCF10A acini is plotted for untreated (white) and Galunisertib-treated cells (gray; n = 12 acini/condition/experiment performed in duplicate). ****p $<10^{-4}$, unpaired t-test with Welch's correction.

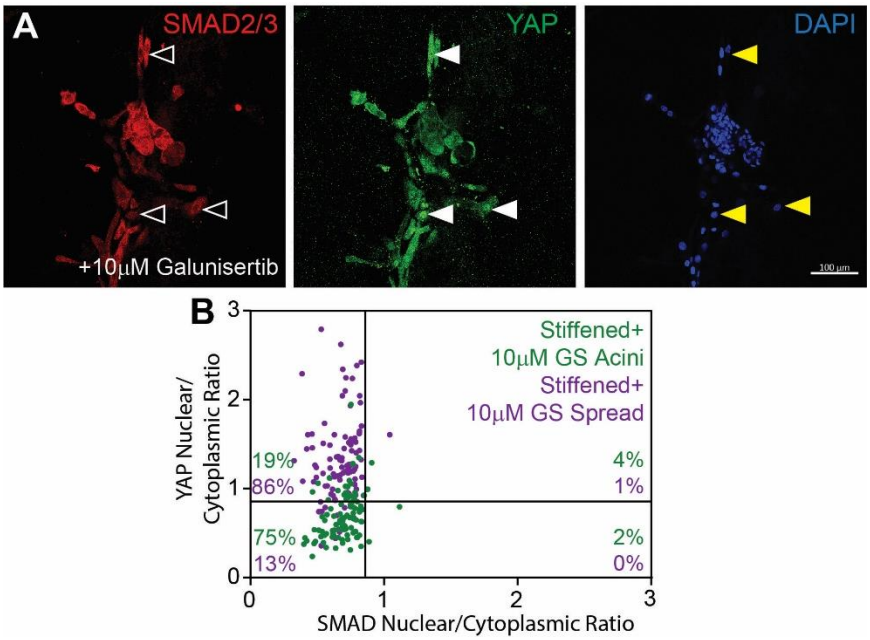

Supplementary Figure 2.11. SMAD inhibition does not prevent YAP nuclear localization
(A) Immunofluorescent images of SMAD2/3 (red) and YAP (green) for MCF10A cells grown on stiffened hydrogels and treated with Galunisertib. Hollow arrowheads indicate cytoplasmic localization of SMAD2/3 and filled arrowheads indicate nuclear localization of YAP. (B) Plot of the nuclear to cytoplasmic intensity ratio for YAP and SMAD2/3 (n=100 cells). Delineated lines indicate cells that are positive or negative for the markers.

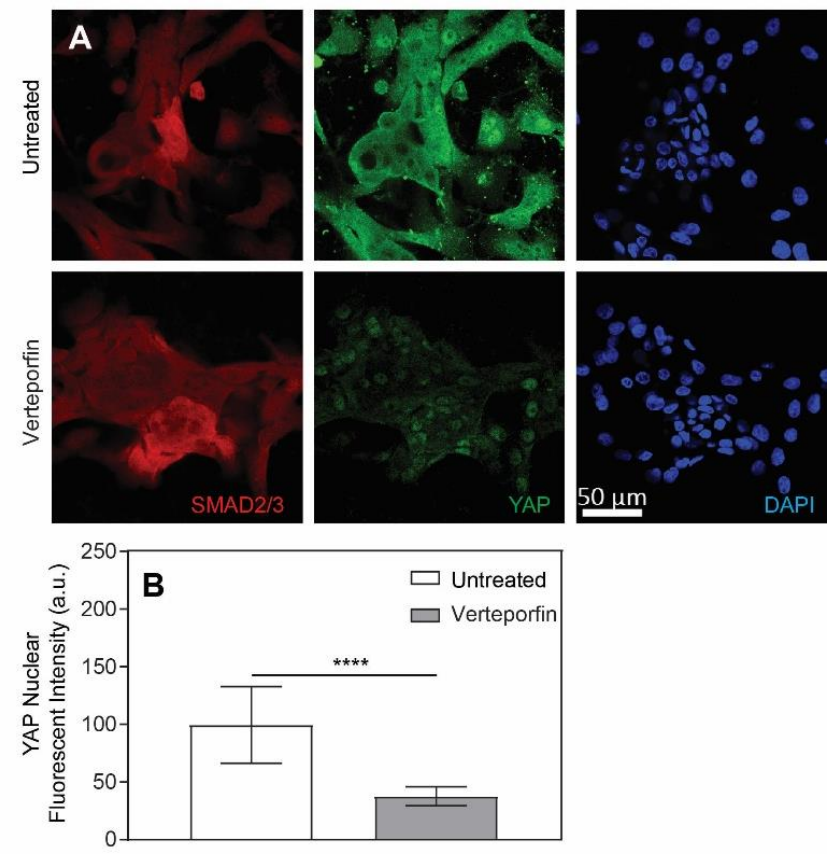

Supplementary Figure 2.12. Verteporfin reduces YAP expression in MECs on stiffened MeHA hydrogels (A) Immunofluorescent images of SMAD (red) and YAP (green) for MCF10A cells grown on stiff hydrogels and treated with Verteporfin. (B) Nuclear intensity of YAP expression in cells with or without Verteporfin added. ****p <0.0001, unpaired t-test with Welch's correction.

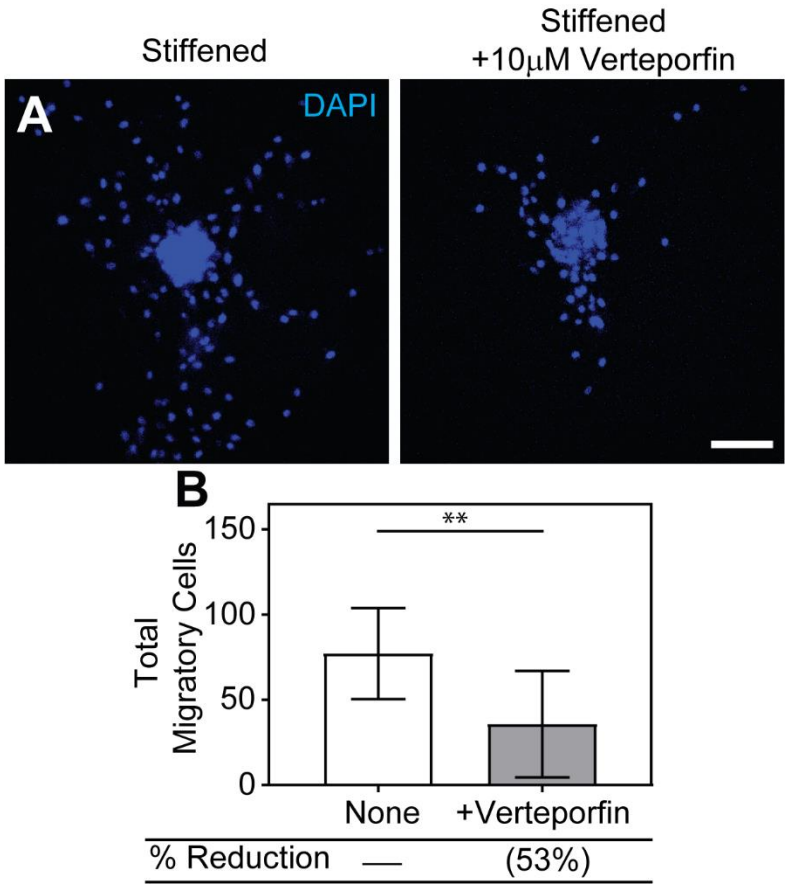

Supplementary Figure 2.13. Verteporfin reduces MECs migration on stiffened MeHA hydrogels
(A) Fluorescent images of cells on stiffened substrates that were selectively treated with Verteporfin after stiffening and stained with Hoechst (blue). (B) The total number of cells migrating out of MCF10A acini is plotted for untreated (white) and Verteporfin-treated cells (gray; n = 12 acini/condition/experiment performed in duplicate). **p <0.01, unpaired t-test with Welch's correction.

2.7 Acknowledgements

The authors would like to thank Dr. Alexander Fuhrmann for assistance in calculating collagen rupture lengths and Elizabeth Bird for assistance in determining MEC substrate adhesion. Funding for this work was provided by National Institutes of Health grants R01CA206880 (A.J.E. and J.Y.), F32HL126406 (J.K.P.), and T32AR060712 (A.K.), Department of Defense grants W81XWH-13-1-0132 (J.Y.) and W81XWH-13-1-0133 (A.J.E.), a National Science Foundation grant 1463689 (A.J.E.) and the Graduate Research Fellowship program (M.G.O. and A.K.), and the ARCS/Roche Foundation

Scholar Award Program in the Life Science (A.K.). Additional fellowship support was provided the Brazilian Federal Agency for Support and Evaluation of Graduate Education award 88881.135357/2016-01 (B.F.M.).

Chapter 2, in full, is a reprint of the material as it appears in Ondeck M, Kumar A, Placone J, Plunkett C, Matte B, Wong K, Fattet L, Yang J, Engler A. Dynamically Stiffening Niche Promote Malignant Transformation of Mammary Epithelial Cells via Collective Mechanical Signaling. Submitted. The Thesis author was the second author of this paper.

Chapter 3.

H-Ras Transformation Attenuates Stiffness Mediated Invasion in Mammary Epithelial Cells

3.1 Abstract

Normal mammary epithelial cells (MECs) are highly responsive to matrix stiffness, undergoing epithelial-to-mesenchymal transition (EMT) with increasing stiffness. However mammary tumors are a complex mixture of MECs with varying phenotypes and mutations and the adjacent stroma ranges from normal mammary stiffness, ~150 Pascal (Pa), to high malignant and stiff, ~5700 Pa. Thus we sought to understand how specific isogenic variants change MEC sensitivity to matrix stiffness. Pre-malignant MCF10A and Ras-transformed MCF10AT were cultured on Matrigel-overlaid polyacrylamide gels ranging from normal mammary stiffness, ~150 Pa, to high malignant and stiff, ~5700 Pa. Though cell were more proliferative and spread at 5700 Pa independent of transformation, only transformed cells exhibited a heterogeneous spread behavior with nuclear localization of the EMT marker TWIST at 150 Pa. Within this heterogeneous population, spread cells exhibited an elongated, mesenchymal-like morphology and disrupted localization of E-Cadherin and basement membrane expression. Stiffness-mediated transformation was blocked by treatment with R-Roscovitine, suggesting an important link between stiffness

sensitivity and intercellular CDK activity. These data suggest that when present, transformed subpopulations may provide an early, pre-fibrotic means for MEC proliferation independent of other microenvironmental cues.

3.2 Introduction

Breast cancer metastasis remains an extremely poor prognostic marker for patient survival associated with nearly a 75% reduction in 5 year survival rate[1]. This process begins with local invasion of cancerous mammary epithelial cells into the adjacent stromal environment and culminates in the formation of distal secondary tumor masses in peripheral tissues such as bone, lungs, liver, and brain[22-24]. Throughout the progression of the tumor toward distal metastasis, extensive remodeling of the tumor microenvironment takes place with increases in fibular collagen and fibronectin as well as increased crosslinking and fiber alignment[56, 58, 78]. Taken together these changes result in an increase in rigidity which is itself a major diagnostic marker: initial detection of breast tumors are often identified through manual palpation of the mass[61].

Cellular mechanotransduction is a fundamental driver of cellular phenotype and behavior in numerous physiological contexts[12]. During development, modulation of stiffness cues have been shown to alter the fate of mesenchymal stem cells between neural, muscle, and bone lineages[51]. In mammary carcinoma, increases in substrate stiffness have been linked with depolarization of mammary acini, increased ERK pathway activity, and ultimately MEC invasion into the microenvironment[14]. Stiffening of the niche can also bring about an epithelial to mesenchymal transition (EMT) through localization of the mechanosensitive basic helix loop helix transcription factor Twist1[79]. However, while

these efforts have focused on alterations to benign mammary epithelial cells (MECs), the tumor niche is a heterogeneous mixture of cells with variable oncogenic mutational status and, as a result, malignancy[101, 102]. Thus we sought to determine how transition from benign to pre-malignant tumor cells affects the sensitivity of a given mammary organoid to stiffness cues. We theorized that, as mutational burden increased, sensitivity to mechanical cues would also increase leading to increased invasive potential at lower, healthier stiffness.

3.3 Results

3.3.1 H-Ras Transformed Mammary Epithelial Cells Show Elevated Stiffness Sensitivity

Elevated microenvironment stiffness has been shown to induce invasive behavior in benign MCF10A MECs which undergo an epithelial to mesenchymal transition mediated by Twist1. To determine whether increasingly malignant MECs show an altered sensitivity to niche stiffness, we cultured three isogenic variants of the MCF10A cell line, H-Ras transformed MCF10AT cells, ductal carcinoma derived MCF10DCIS cells, and metastatic MCF10CA1 cells, on polyacrylamide hydrogels ranging from physiologically soft (~150Pa) to pathologically stiff (~5700Pa) conditions. All cell lines showed organoid destabilization and increased invasive behavior with increasing stiffness (Supplemental Figure 3.1A). However, while most lines including benign MCF10A cells showed a transition between phenotype near 670Pa, the H-Ras transformed MCF10AT cells spread into the surrounding stroma at all stiffness conditions including 150Pa (Figure 3.1A).

These cells also showed an overall reduction in the number of stable organoids as well as an increase in the number of invasive cells leaving the organoids into the surrounding

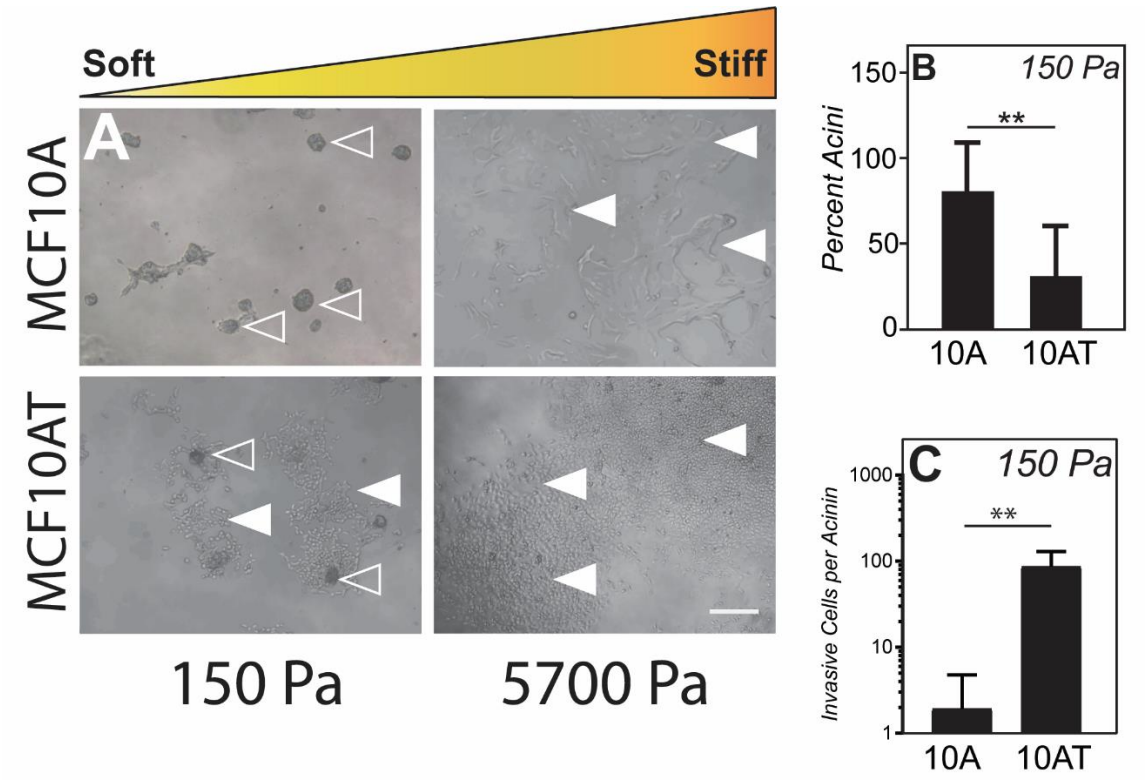

Figure 3.1. H-Ras transformed cells show partial-invasive behavior at philologically soft mammary stiffness. **(A)** Bright field images of MECs cultured on PA substrates. Hollow arrows indicated acini while solid arrows indicate spread regions. Scale Bar 250μm. **(B)** Total percentage of acini present per hydrogel at low stiffness for each MEC line. n=1 hydrogel (~10 acini) per biological replicate, 3 biological replicates per condition. Mean±S.D. $^{**}p<0.01$ **(C)** Average number of invasive cells produced per acini. n=4 acini per biological replicate, 3 biological replicate per condition. Mean±S.D. $^{**}p<0.01$, non-paired t test with Welch's correction.

stroma (Figure 3.1B, C). Morphological assessment of cell circularity also showed a gradual conversion from round to elongated phenotypes in MCF10A, MCF10DCIS, and MCF10CA1a cell lines as substrate stiffness increased but MCF10AT cells showed partial elongation even in soft gel cultures (Supplemental Figure 3.1B). These data outline a heightened stiffness sensitivity in H-Ras mutant cells when compared to their isogenic variants which in turn induces a heightened invasive phenotype not observed in benign MECs.

3.3.2 H-Ras Transformed Cells Adopt a Heterogeneous Phenotype in a Soft Microenvironment

Cellular invasion of mammary stroma in stiff environmental conditions has been associated with an Epithelial to Mesenchymal transition whereby invading cells lose junctional and basement membrane stability, adopt an elongated morphology, and upregulate secondary fiber expression. To explore whether the invasive cell population adopts this EMT phenotype, we examined E-Cadherin and basement membrane expression in the four isogenic cell lines on soft (150Pa) and stiff (5700Pa) hydrogels. All cell lines showed loss of the basement membrane protein Laminin V as well as disruption of E-Cadherin localization in stiff conditions (Figure 3.2A, Supplemental Figure 3.2A). Corresponding with previous results, when cultured on soft substrates, the invasive fraction MCF10AT derived organoids showed destabilization of basement membrane and partial loss of E-Cadherin localization (Figure 3.2A right panels). Morphological analysis of MCF10AT cells when cultured on soft substrates also suggested a heterogeneous phenotype with some cells remaining polarized and others beginning to spread and elongate (Figure 3.2B). Taken together, these data suggest the adoption of a partial EMT-phenotype among a subset of spreading H-Ras mutant cells despite a soft environmental condition.

To further explore the upstream activators of this partial EMT phenotype, we performed real time PCR analysis on five key transcription factors associated with EMT. Of the five none showed significant variation in expression levels between groups (Supplemental Figure 3.2B). However, it has been previously noted that transcriptional activity of Twist1 is mediated by nuclear localization. To explore this means of EMT

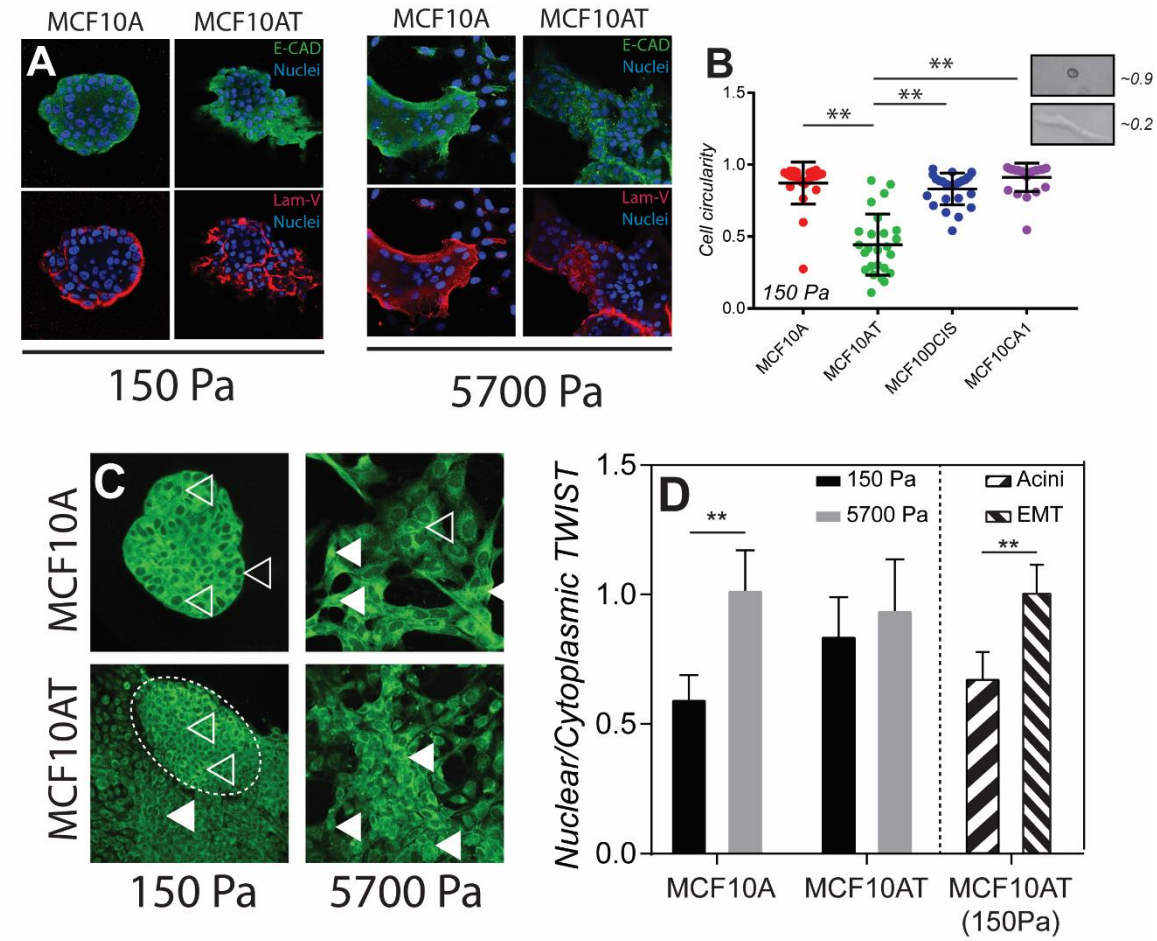

Figure 3.2. Invasive subpopulations of H-Ras transformed cells undergo EMT in a low stiffness environment. Mutation and niche stiffness can induce a mesenchymal phenotype in spreading cells. **(A)** IF staining for E-Cadherin (green), Laminim V (red) and DAPI. **(B)** Distribution of cell circularity on soft (~150 Pa) substrates shows heterogeneous morphology among H-Ras mutant mammary cells. Circularity of 1 corresponds to a perfect circle while circularity of 0 corresponds to a linear structure. n=8 cells per biological replicate, 3 biological replicates per condition Mean±S.D. **p<0.01, one-way ANOVA with multiple comparisons. **(C)** IF staining of TWIST1 where hollow arrows indicate non-nuclear localizing transcription factor while solid arrows indicate localized transcription factor. **(D)** TWIST nuclear-to-cytoplasmic fluorescent intensity ratio. Right striped bars show the ratio for MCF10AT cells in acinar (left bar) or mesenchymal-like structures (right bar) on 150 Pa hydrogels. Mean±S.D. **p<0.01, non-paired t test with Welch's correction.

activation, we performed immunofluorescent confocal microscopy. Twist1 localization was observed in in stiff conditions in all four cell lines (Figure 3.2C, Supplemental Figure 3.2C). However, MCF10AT cells adopted a heterogeneous behavior with organoid regions remaining non-localized and spread regions localizing the protein (Figure 3.2C-D). Interestingly, despite the noted role of the signaling molecule TGF-β in induction of EMT,

there was not a corresponding increase in TGF-β mediated SMAD2/3 localization within the spread region implying an independent mechanism (Supplemental Figure 3.3). As such, we demonstrate that, unlike in benign MECs, the EMT subpopulation of invasive H-Ras transformed cells remains Twist1 mediated despite the apparent lack of a biophysical stiffness cue.

3.3.3 Cyclin Dependent Kinase Activity Regulates Stiffness Sensitivity

Among the noted baseline differences between MCF10A and MCF10AT cell lines was a noted increase in proliferation among 10AT cells. Noting this, we chose to explore the role of cyclin dependent kinases (CDKs), key regulators in cell cycle progression, in altering stiffness sensing mechanisms. To observe the dependencies of local invasion on CDK activity, we treated pre-formed organoids seeded on soft and stiff hydrogels with R-Roscovitine, a small molecule CDK and cell cycle inhibitor. Treatment of organoids with Roscovitine resulted in total loss of EMT behavior in H-Ras transformed spheroids on soft substrates (Figure 3.3A, Bottom Left). Interestingly, this treatment also prevented spreading on pathologically stiff substrates for both benign and H-Ras transformed cells (Figure 3.3A, Right). Invasive cell area per organoid was significantly reduced in all stiff conditions as well as for H-Ras transformed cells on soft substrates (Figure 3.3B). While these findings were extremely interesting, because Roscovitine is a broad spectrum CDK inhibitor, it was not clear which protein was chiefly responsible for mediating stiffness sensitivity. In order to narrow the number of potential targets for this stiffness regulatory mechanism, we have begun to assess the relative expression levels of the R-Roscovitine targets through RT-qPCR. Preliminary results show trending increases in CDK5 across H-Ras mutant and stiff conditions suggesting a possible upregulation of the protein (Figure

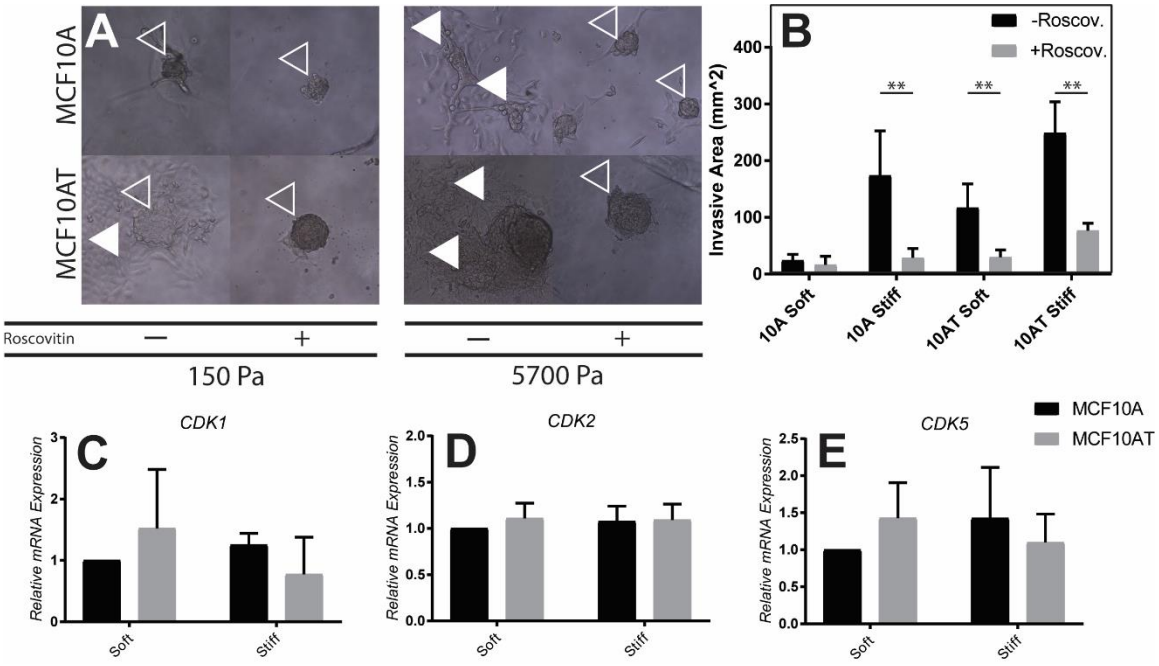

Figure 3.3. Cyclin Dependent Kinase Activity Mediates Stiffness Sensitivity in MEC Organoids
(A-B) Inhibition of Cyclin Dependent Kinases 1, 2, and 5 suppresses stiffness mediated invasion. **(A)** Bright field images of MEC spheroids untreated (-) or treated (+) with 10μM Roscovitine. Hollow arrows indicate acini while solid arrows indicate spreading. **(B)** Quantification of spread cell area per acinus for treated and untreated MECs. n=6 technical replicates, 2 biological replicates per condition. Mean±S.D. **p<0.01 two-way ANOVA with multiple comparisons. **(C-E)** CDK expression trends upward in stiff and H-Ras transformed conditions. RT-qPCR analysis of CDK1 **(C)**, CDK2 **(D)**, and CDK5 **(E)** between soft, stiff, benign, and H-Ras transformed cell lines. n=3 biological replicates per condition. Mean±S.D.

3.3C-E). Taken together, these results shows a complete CDK mediated knockdown of stiffness sensitivity in multiple mammary epithelial cell lines as well as potential upregulation of CDK5 in invasive cell populations highlighting an important role for cell cycle regulators in MEC stiffness transduction.

3.4 Conclusion

Here, we have demonstrated that H-Ras transformed MECs show elevated stiffness sensitivity when compared to benign isogenic counterparts. H-Ras transformed cells adopted a partially invasive phenotype on substrates with physiologically healthy stiffness. This invasive cell fraction also appeared to undergo a partial EMT allowing for increased

migratory and proliferative capacity. These findings suggest that, as tumors continue to develop and accumulate oncogenic mutation, the sensitivity of malignant cells may drive premature invasive behavior. The presence of certain oncogenes, such as H-Ras, within a tumor may therefore offer a predictive metric for assessing the likelihood of regional or distal metastasis. It is therefore of great importance to identify and explore the role of other key mammary cell mutations such as BRACA1, B-RAF, or PI3K in altering stiffness sensitivity. These mutations may, through a similar mechanism, sensitize tumor masses to stiffness and allow for rapid destabilization and spreading.

In exploring the proliferative differences between H-Ras transformed and benign cells, we have identified a potential role for cell cycle regulators such as CDKs in modulating the stiffness sensitivity of MECs. Given that the effect of CDK regulation of stiffness sensation was observed in both benign and H-Ras transformed cell lines, it is likely that both H-Ras and CDKs act separately to modulate cellular invasion and organoid destabilization. While the mechanism for this signaling remains undefined, recent work exploring the role of CDK5 in promoting EMT in mammary cells suggests a potential link between CDK activity and focal adhesion stability mediated by phosphorylation of focal adhesion kinase. Given that focal adhesions are the principle transducers of physical ECM cues to the cytoskeleton, an interplay between CDK activity and focal adhesion assembly provides a promising path forward for this mechanistic analysis.

3.5 Methods

3.5.1 Polyacrylamide Hydrogel Synthesis

Polyacrylamide gels were prepared on 12mm glass coverslips as previously described[103]. Coverslip surfaces were cleaned by 5 minute UV-Ozone treatment then immediately functionalized with 3-(trimethoxysilyl)propyl methacrylate (Sigma-Aldrich) and rinsed with 100% EtOH. Solutions of acrylamide/bis-acrylamide were mixed with 10% ammonium persulfate () and Tetramethylethylenediamine (Fisher Scientific) at a ratio of 1000:10:1 respectively and was allowed to polymerize between a functionalized slip and a glass slide coated in dichlorodimethylsiloxane (Sigma-Aldrich). Polymerized gels were then washed with PBS and incubated with 0.2mg/mL Sulfo-SANPAH () in 50mM HEPES pH 8.5 in the presence of 360nm UV light for 10 minutes, rinsed twice with PBS, and finally incubated overnight at 37°C with rat tail Collagen I (Millipore) in dH20. Gels were then rinsed with PBS and sterilized prior to use.

3.5.2 Cell Culture

MCF10A, MCF10AT, and MCF10DCIS cells were grown in DMEM/F12 media containing 5% Horse Serum, 20ng/mL human EGF, 0.5mg/mL hydrocortisone, 100ng/mL cholera toxin, 10ug/mL insulin, and 1% penicillin and streptomycin. MCFCA1 cells were grown in DMEM/F12 media containing 5% horse serum and 1% penicillin and streptomycin.

3.5.3 3-Dimensional Cell Culture

All cell lines were seeded on hydrogels in the presence of 2% Matrigel (Corning) mixed with DMEM/F12 supplemented with 2% horse serum, 5ng/mL human EGF, 0.5mg/mL hydrocortisone, 100ng/mL cholera toxin, 10ug/mL insulin and 1% penicillin and streptomycin. Single cells were seeded on hydrogels at a density of 2000 cells per gel

and allowed to for mammary organoids for 6 days in culture. For pre-formed organoids, cells were added to pre-rinsed Aggrewell 400 plates (Stem Cell Technologies cat #34411) at density of approximately 200 cells per spheroid in a mixture of media and 0.25% Methocult (Stem Cell Technologies, cat # H4434). Spheroids were allowed to form over a four day period, removed and re-seeded onto hydrogels in the presence of 2% Matrigel. Pre-formed organoids were treated with small molecule inhibitors immediately after seeding on hydrogels at the following concentrations: Roscovitine (Cell Signaling Technologies, 15μM).

3.5.4 Confocal Microscopy

Cells were fixed with 3.7% formaldehyde for 15 minutes at room temperature. Matrigel was removed from samples by incubation in 5mM EDTA (Fisher, cat# BP20-1) for 30 minutes at 4°C. Samples were then permeablized with PBS supplemented with 2M MgCl2 (Solution A) and 0.5% Triton X-100 () for 15 minutes at room temperature. Sample blocking was performed in a solution of 20% goat serum and 0.2% Triton-X 100 in Solution A for 30 minutes at room temperature. Primary antibodies were added and incubated overnight at 4°C. Dilutions were as follows: Anti-E-Cadherin (1:250), Laminin V (abcam, ab11575, 1:100), TWIST1 (Santa Cruz Biotechnology, sc-81417, 1:25), SMAD2/3 (Cell Signaling Technology, D7G7, 1:1600), YAP (Santa Cruz Biotechnology, sc-101199, 1:50). Samples were washed three times with Solution A for 5 minutes and subsequently incubated in secondary antibody solution (Solution A +0.2% TritonX-100 +20% Goat Serum) at the following dilutions: Goat anti-mouse 488 (Invitrogen, A11004, lot 1218263), Goat anti-rabbit 568 (A11011, Lot 1345045) for 1 hour at room temperature. Samples were again washed three times for 5 minutes with Solution A and Nuclei were

counterstained with DAPI (1:5000) in dH2O for 3 min. Hydrogels were mounted to glass slides using Fluoromount-G (Southern Biotech, cat# # 0100-01) and allowed to rest for 1 hour after which gels were sealed with clear nail polish.

3.5.5 Image Processing

Bright field images were acquired on a Nikon Eclipse Ti-S inverted microscope with a 10x objective. Images were analyzed in ImageJ software. Organoid margins and invasive cell area were traced and quantified by the software operator while cell circularity was derived from the equation Circularity=4π area/〖perimeter〗^2 . Cell counts were performed using custom ImageJ code for particle analysis. Confocal images were taken on a Zeiss LSM 780 with a 40x water immersion objective. Images were linearly analyzed in ImageJ and Zen software packages. Nuclear to cytoplasmic intensity ratios were calculated through the following method. Average nuclear fluorescent intensity was identified for an individual cell and subsequently normalized to the same cell's average cytoplasmic fluorescent intensity. This process was carried out in both "Acini" and "EMT" regions as determined by the software operator.

3.5.6 Subpopulation Isolation

To separate acini and spread cell regions, gels were mechanically dissected using a Zeiss Stereo Discovery.V8 for visualization. Resection of organoids was performed using a microdissection scalpel as described in Supplemental Figure 3.4. Organoids and spread cell regions utilized in the phenotype stability assay were then exposed to 0.05% Trypsin for 5 minutes and re-seeded on soft polyacrylamide gels as previously described.

3.5.7 qPCR

RNA was isolated from samples using a guanidinium thiocyanate-phenol-chloroform extraction (TRIzol). CDNA was synthesized using SuperScript III reverse transcriptase (Thermo Fisher Scientific) with random hexamer primers. Quantification was carried out on a CFX384 Touch RT-PCR system (BioRad) with a SYBR Green probe (Thermo Fisher Scientific). All samples were run in technical triplicate and normalized to GAPDH.

3.6 Supplementary Figures

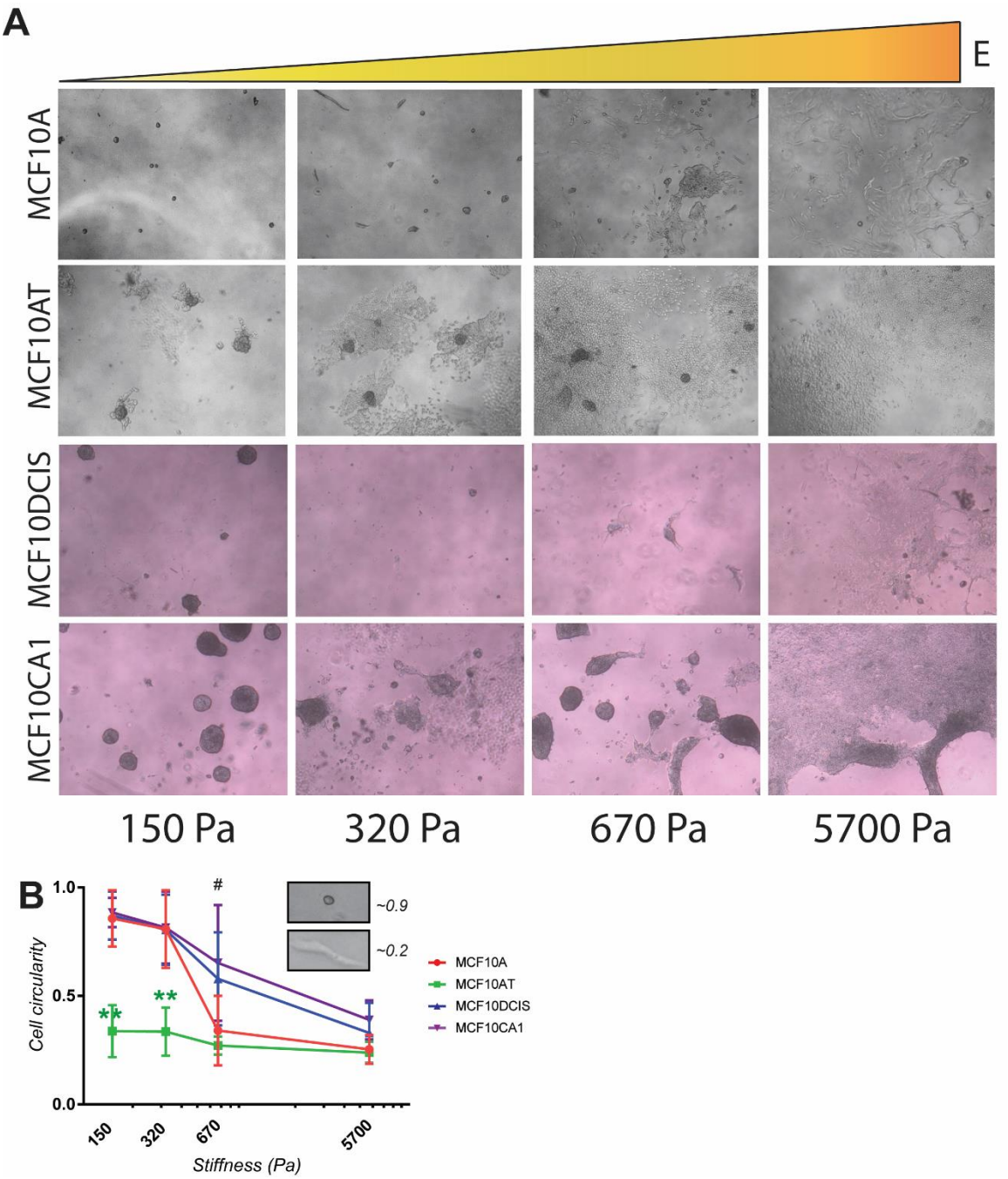

Supplementary Figure 3.1. MEC sensitivity to stiffness is gradual and varies between isogenic variants. **(A)** Bright field images of MCF10A, MCF10AT, MCF10DCIS, and MCF10CA1a cell lines when cultured on incrementally stiffer gels. **(B)** Cell circularity measurements for cell lines at stiffness ranging from 150 Pa to 5700 Pa. Circularity of 1 corresponds to a perfect circle while circularity of 0 corresponds to a linear structure. n=8 cells per biological replicate, 3 biological replicates per data point per condition. Mean±S.D. **p<0.01, one-way ANOVA with multiple comparisons.

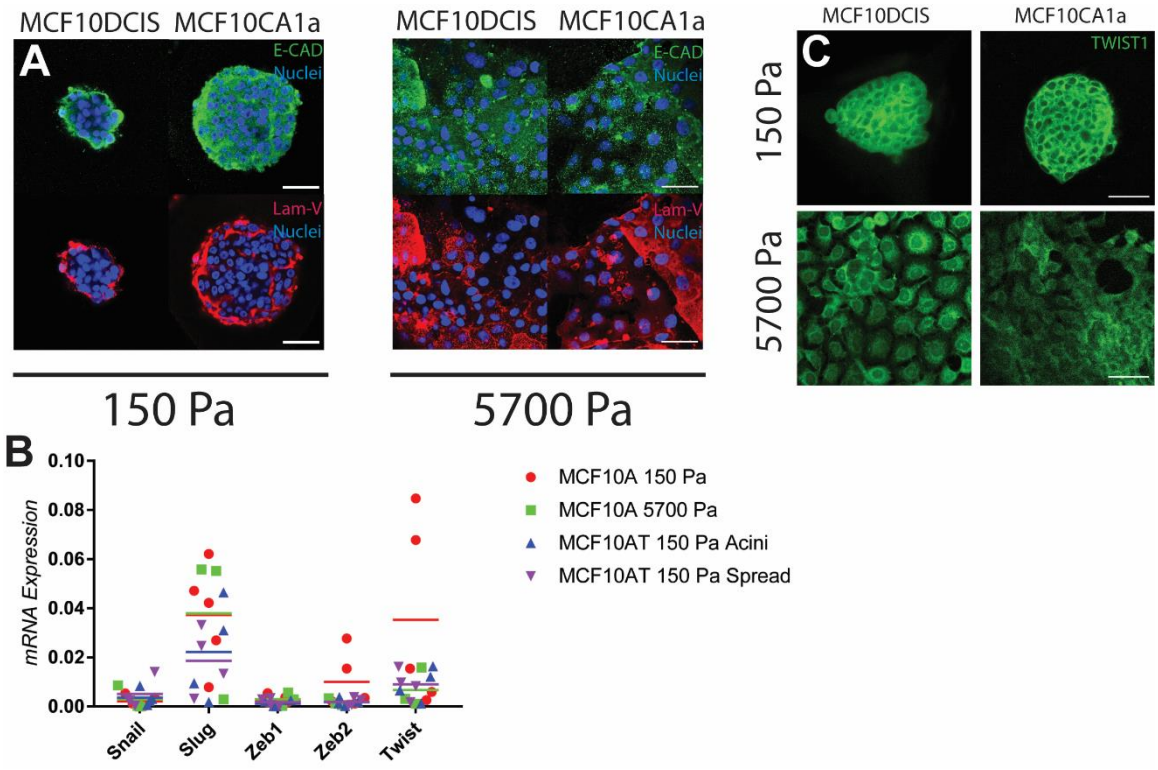

Supplementary Figure 3.2. MEC sensitivity to stiffness is gradual and varies between isogenic variants. **(A)** IF staining for E-Cadherin (green), Laminim V (red) and DAPI. Scale bar=250μm **(B)** RT-qPCR analysis of EMT inducing transcription factor mRNA expression for Snail1, Slug, Zeb1, Zeb2, and Twist1. n=4 biological replicates per condition. Mean±S.D. **(C)** IF staining of TWIST1 in MCF10DCIS and MCF10CA1a cell lines. Scale bar=250μm.

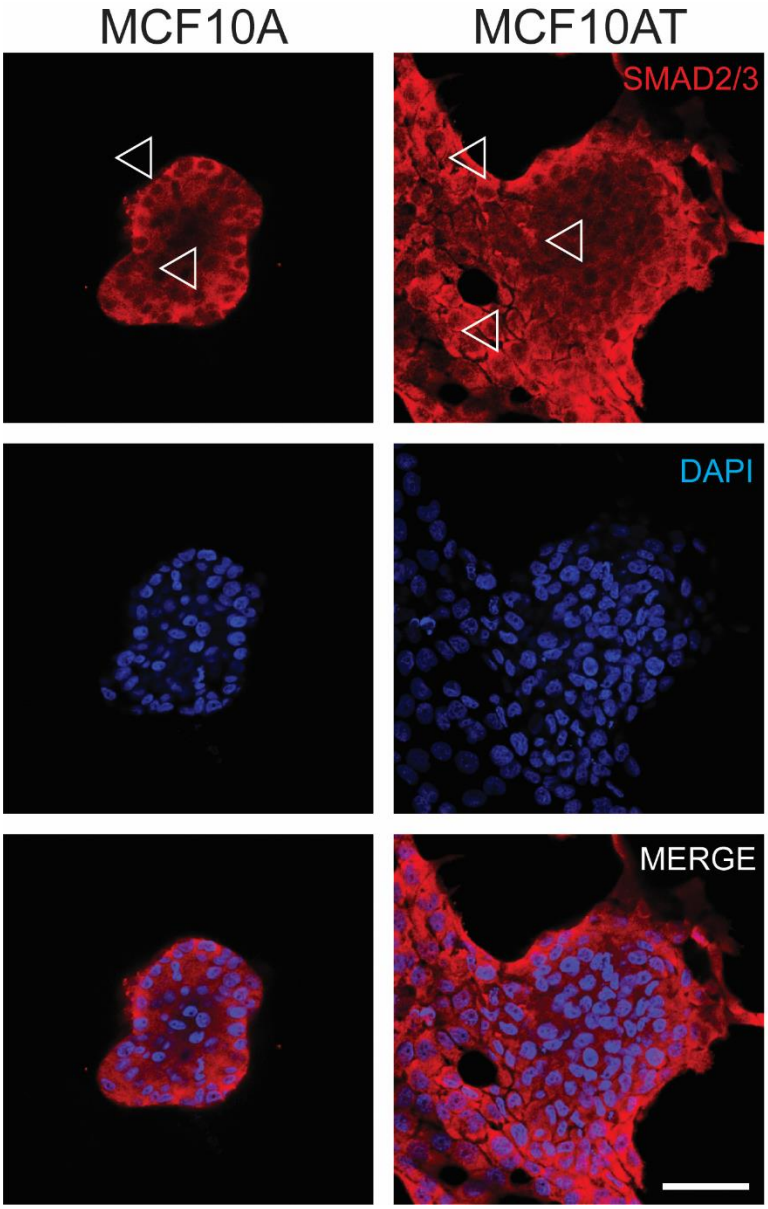

Supplementary Figure 3.3. SMAD2/3 localization does not favor invasive cells on soft substrates.
IF images of SMAD2/3 (red) localization and DAPI in MCF10A and MCF10AT cell cultures on soft (~150Pa) substrates. Hollow arrowheads indicate non-nuclear localized cells. Scale bar=250μm.

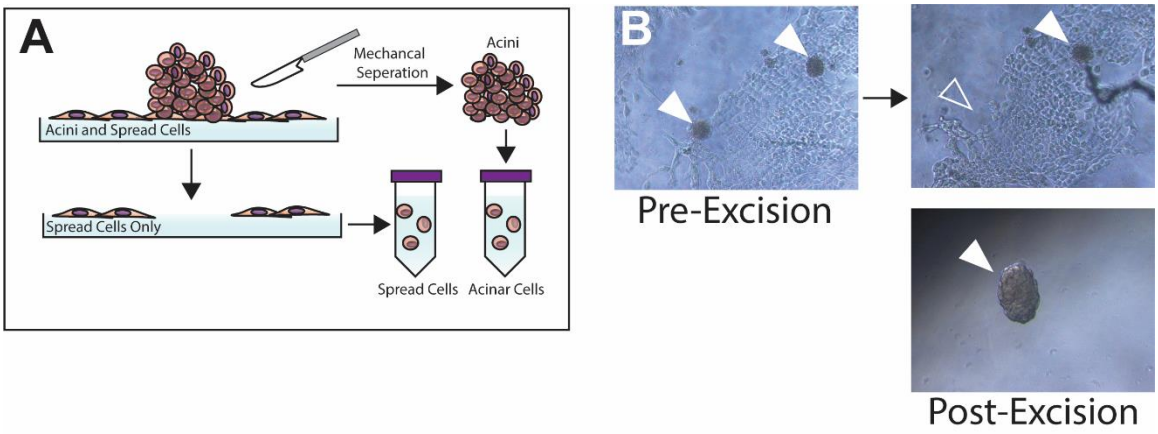

Supplementary Figure 3.4. Separation of spread and acinar fractions of H-Ras transformed cells
(A) Graphical abstract of the separation protocol utilized to analyze spread and acinar fractions of MCF10AT cells when cultured on soft substrates. Mechanical resection with a microdissection blade under a low magnification dissection microscope was employed to isolate acini from hydrogels. Spread regions are then separated similarly and both fractions are purified for biochemical assay. **(B)** Validation of the separation of acini from soft gels. Solid arrows denote acinar regions while the hollow arrow denote the location where acini have been removed.

3.7 Acknowledgements

Funding for this work was provided by National Institutes of Health grants R01CA206880 (A.J.E. and J.Y.), the Graduate Research Fellowship program (A.K.), and the ARCS/Roche Foundation Scholar Award Program in the Life Science (A.K.).

Chapter 4.

Conclusions

4.1 Introduction

The complex interplay of environmental cues and genetic or proteomic changes to cells within the tumor niche presents a unique and paradoxical challenge to those who wish to study disease progression. In vivo studies, while comprehensive in the diversity of cues, signals, and substrate properties, often lack the detail or nuance to probe the role of any one specific factor and elucidate its role. However, opting for a more regulated in vitro approach often oversimplifies the disease and observations may not be consistent with the reality of the disease pathophysiology. Thus is it is imperative that sophisticated and well defined model systems be generated, utilized, and improved to better approximate actual disease phenotypes. In this Thesis document, I have outlined the results from two such model optimizations: dynamically stiffening substrates to model progressive fibrosis of the tumor niche, and variably malignant cell type to model accumulating oncogene mutational burden within a tumor and its effect on stiffens sensitivity. Both have revealed new insights into the complexity of mechanisms employed by tumor cells to invade into the surrounding stromal environment. These and future studies will further refine our understanding of tumor progression from low to high grade and, hopefully, identify novel target mechanisms for the inhibition of invasive metastatic behavior.

4.2 Dynamic Stiffening Promotes Partial Invasion in Benign Mammary Epithelial Cells Mediated by YAP and SMAD

Traditionally, studies meant to explore the role of stiffness changes in the tumor microenvironment on promoting invasion focus on static stiffness conditions (i.e. soft and healthy versus stiff and tumorigenic). While certainly useful in many contexts, this analysis lacks the progressive nature of tumor development. Patients are not born with stiff tissue but rather tissue is remodeled from a soft to stiff state. Thus we sought to determine what role the *transition* from soft to stiff substrate had on invasive potential. To do this we employed the use of a methacrylated hyaluronic acid hydrogel that could be dynamically stiffened through brief UV exposure to simulate the conversion from a soft to stiff microenvironment. Acini cultured on this substrate underwent a partial-EMT with select cells opting to spread into the surrounding stroma while others remained polarized and within the acinus. This behavior was, in part, mediated by both SMAD2/3 activation and YAP nuclear localization with dual inhibition of these intermediates synergizing to drastically reduce the number of invasive cells. This study provides a new and exciting departure from traditional static gel based methods. YAP activation, for example, was not found in previous work to play a definitive role in a similar but static polyacrylamide based hydrogel model which conflicts with its widely established link to cancer mechanosensing. Thus cell behavior is modulated by both its current and prior environmental state highlighting the importance of simulating developmental conditions when exploring mammary carcinomas.

4.3 Increased Malignancy Alters the Stiffness Sensitivity of Mammary Epithelial Cells

While substrate stiffness has been shown to impact benign mammary epithelium, it was not known how transition to a pre-malignant state would alter cellular behavior on a stiffened substrate. One would expect that the accumulation of activated oncogenes may lead to an increased sensitivity to stiffen of the overall mass. To explore how increasingly malignant cell types responded differentially to substrate stiffness, we opted to utilize the isogenic variants of the MCF10A cell line. While the in vivo passaged lines (MCF10DCIS and MCF10CA1) showed no variation from MCF10A behavior, the H-Ras mutant MCF10AT cell line adopted a partial EMT phenotype even on a physiologically soft gel (~150Pa). This partial phenotype showed differential regulation of hallmark EMT markers such as E-Cadherin as well as differential localization of the stiffness responsive transcription factor Twist. Proliferative differences mediated by cyclin dependent kinase activity was found to be a key mediator in this partial phenotype as CKD knockdown through treatment with R-Roscovitine resulted in the loss of any spreading behavior in all conditions. Thus the interplay of constitutively active H-Ras coupled with CDK mediated invasion may induce an overall increased sensitivity to substrate stiffness in pre-malignant cell types. Broadly speaking, this study attempts to explore a temporal snapshot of the stage 0 tumor state following ductal carcinoma but prior to invasion and metastasis. It is at this inflection point that patient outcomes begin to sharply decline and, as such, it is important to determine the contributing factors such as stiffness sensitivity toward this change in phenotype.

4.4 Future directions

The work outlined here attempts to approximate the temporal nature of tumor progression as it moves from an early stage 0 to stage 4 carcinoma. While these model systems have provided insights into cellular behavior in the niche, there is still room to expand the scope of this analysis. For example, the tumor niche does not, as simulated in Chapter 2, undergo near immediate crosslinking. Rather it gradually stiffens over the course of several months or years. This altered rate of stiffening likely impacts the overall junctional instability observed in our dynamic model which can in turn suppress YAP localization through LATS1/2 regulation. As such, a proposed future study would explore a gradual stiffening of the niche over a longer period of time through sequential stiffening events (Figure 4.1). By modulating the degree and rate of remodeling in the niche, we may begin to understand the relationship between slow or rapid environmental remodeling (dictated largely by cancer associated fibroblasts within the niche) and the severity of the cancer.

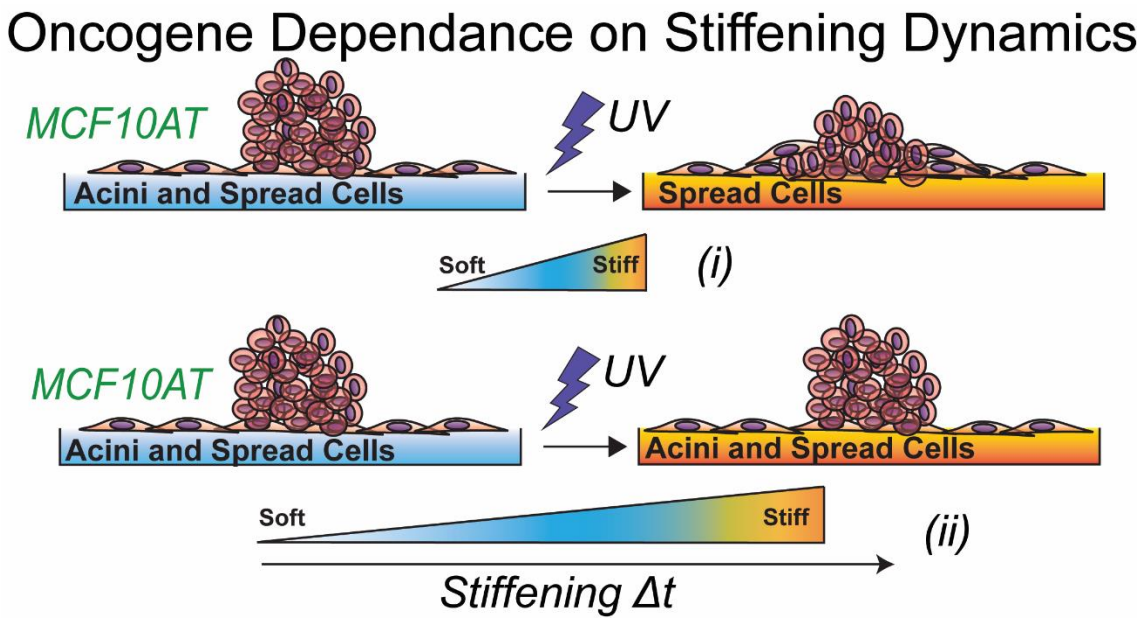

Figure 4.1. Proposed study of modulated stiffening time and effects on MEC cell lines.
Graphical abstract of the proposed study of rapid and gradual stiffening events on the spreading behavior of MECs. (i) Rapid stiffening from physiologically soft (~100Pa) to pathologically stiff (~3000Pa). (ii) Gradual stiffening over the same regime through multiple, short UV intervals to simulate remodeling of the tumor microenvironment *in vivo*.

Another temporally motivated study is the gradual accumulation of mutational burden within a tumor mass. While we have approximated this through use of the H-Ras transformed MCF10AT cell line, organoids formed from these cells do not adopt a stable acinus as with their benign isogenic parent line. Furthermore, isogenic comparisons such as the 10AT line are limited in the mutations that can be studied. As such there is a need for a cell line that is both versatile in its mutational profile and that can be dynamically reprogramed from a benign to malignant state *in situ*. Genetic technologies such as the TET-Doxycycline and inducible CRISPR/CAS9 can provide the means to accomplish both of these goals with a host of oncogene targets (Figure 4.2). Indeed a TET system has been developed previously for the MCF10A cell line targeting the B-RAF oncogene. Conditional expression of oncogenes including B-RAF, BRACA, H-RAS, and PI3K may all be studied with such as system. By combining dynamic genome alterations through

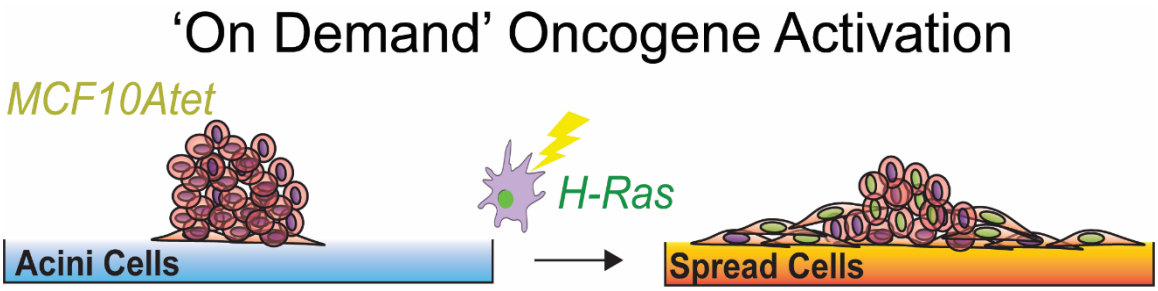

Figure 4.2. Proposed Study of Inducible Oncogene Activation.
MCF10Atet transfected cells activate conditional expression of H-Ras with the addition of doxycycline to cell culture media. Transfection efficiency may be modulated to estimate heterogeneous mixtures of TET (green) and wild type (purple) cells. Platform may be used for other inducible oncogenes such as B-RAF, PI3K, or BRACA1 and combined with dynamically stiffening gel to fully assess temporal stiffening and mutation accumulation.

TET switches with dynamic environmental changes through the stiffening hydrogels, we may uncover many yet unknown mechanisms of action involved in invasion that are as of yet unknown.

References

1. Siegel, R.L., Miller, K.D. & Jemal, A. Cancer statistics, 2017. *CA: a cancer journal for clinicians* **67**, 7-30 (2017).

2. Lauby-Secretan, B., Scoccianti, C., Loomis, D., Benbrahim-Tallaa, L., Bouvard, V., Bianchini, F. & Straif, K. Breast-cancer screening—viewpoint of the IARC Working Group. *New England journal of medicine* **372**, 2353-2358 (2015).

3. Lieben, L. Immunotherapy: keeping breast cancer in check. *Nature Reviews Cancer* **17**, 454 (2017).

4. Saadatmand, S., Bretveld, R., Siesling, S. & Tilanus-Linthorst, M.M. Influence of tumour stage at breast cancer detection on survival in modern times: population based study in 173 797 patients. *Bmj* **351**, h4901 (2015).

5. Fossati, R., Confalonieri, C., Torri, V., Ghislandi, E., Penna, A., Pistotti, V., Tinazzi, A. & Liberati, A. Cytotoxic and hormonal treatment for metastatic breast cancer: a systematic review of published randomized trials involving 31,510 women. *Journal of clinical oncology : official journal of the American Society of Clinical Oncology* **16**, 3439-3460 (1998).

6. Weigelt, B., Peterse, J.L. & Van't Veer, L.J. Breast cancer metastasis: markers and models. *Nature reviews. Cancer* **5**, 591 (2005).

7. Scully, O.J., Bay, B.-H., Yip, G. & Yu, Y. Breast cancer metastasis. *Cancer Genomics-Proteomics* **9**, 311-320 (2012).

8. Slamon, D.J., Leyland-Jones, B., Shak, S., Fuchs, H., Paton, V., Bajamonde, A., Fleming, T., Eiermann, W., Wolter, J. & Pegram, M. Use of chemotherapy plus a monoclonal antibody against HER2 for metastatic breast cancer that overexpresses HER2. *New England Journal of Medicine* **344**, 783-792 (2001).

9. Creighton, C.J., Chang, J.C. & Rosen, J.M. Epithelial-mesenchymal transition (EMT) in tumor-initiating cells and its clinical implications in breast cancer. *Journal of mammary gland biology and neoplasia* **15**, 253-260 (2010).

10. Herbertz, S., Sawyer, J.S., Stauber, A.J., Gueorguieva, I., Driscoll, K.E., Estrem, S.T., Cleverly, A.L., Desaiah, D., Guba, S.C. & Benhadji, K.A. Clinical development of galunisertib (LY2157299 monohydrate), a small molecule inhibitor of transforming growth factor-beta signaling pathway. *Drug design, development and therapy* **9**, 4479 (2015).

11. Rodón, J., Carducci, M., Sepulveda-Sánchez, J.M., Azaro, A., Calvo, E., Seoane, J., Braña, I., Sicart, E., Gueorguieva, I. & Cleverly, A. Pharmacokinetic, pharmacodynamic and biomarker evaluation of transforming growth factor-β

receptor I kinase inhibitor, galunisertib, in phase 1 study in patients with advanced cancer. *Investigational new drugs* **33**, 357-370 (2015).

12. Wang, J.H.-C. & Thampatty, B.P. An introductory review of cell mechanobiology. *Biomechanics and modeling in mechanobiology* **5**, 1-16 (2006).

13. Lance, A., Yang, C.C., Swamydas, M., Dean, D., Deitch, S., Burg, K.J. & Dréau, D. Increased extracellular matrix density decreases MCF10A breast cell acinus formation in 3D culture conditions. *Journal of tissue engineering and regenerative medicine* **10**, 71-80 (2016).

14. Paszek, M.J., Zahir, N., Johnson, K.R., Lakins, J.N., Rozenberg, G.I., Gefen, A., Reinhart-King, C.A., Margulies, S.S., Dembo, M. & Boettiger, D. Tensional homeostasis and the malignant phenotype. *Cancer cell* **8**, 241-254 (2005).

15. Debnath, J., Mills, K.R., Collins, N.L., Reginato, M.J., Muthuswamy, S.K. & Brugge, J.S. The role of apoptosis in creating and maintaining luminal space within normal and oncogene-expressing mammary acini. *Cell* **111**, 29-40 (2002).

16. Debnath, J., Muthuswamy, S.K. & Brugge, J.S. Morphogenesis and oncogenesis of MCF-10A mammary epithelial acini grown in three-dimensional basement membrane cultures. *Methods* **30**, 256-268 (2003).

17. Yamada, K.M. & Cukierman, E. Modeling tissue morphogenesis and cancer in 3D. *Cell* **130**, 601-610 (2007).

18. Weigelt, B., Ghajar, C.M. & Bissell, M.J. The need for complex 3D culture models to unravel novel pathways and identify accurate biomarkers in breast cancer. *Advanced drug delivery reviews* **69**, 42-51 (2014).

19. Poller, D., Barth, A., Slamon, D.J., Silverstein, M., Gierson, E., Coburn, W., Waisman, J., Gamagami, P. & Lewinsky, B. Prognostic classification of breast ductal carcinoma-in-situ. *The lancet* **345**, 1154-1157 (1995).

20. Silver, S.A. & Tavassoli, F.A. Mammary ductal carcinoma in situ with microinvasion. *Cancer: Interdisciplinary International Journal of the American Cancer Society* **82**, 2382-2390 (1998).

21. Ma, X.-J., Salunga, R., Tuggle, J.T., Gaudet, J., Enright, E., McQuary, P., Payette, T., Pistone, M., Stecker, K. & Zhang, B.M. Gene expression profiles of human breast cancer progression. *Proceedings of the National Academy of Sciences* **100**, 5974-5979 (2003).

22. Allred, D., Mohsin, S. & Fuqua, S. Histological and biological evolution of human premalignant breast disease. *Endocrine-related cancer* **8**, 47-61 (2001).

23. Gupta, G.P. & Massagué, J. Cancer metastasis: building a framework. *Cell* **127**, 679-695 (2006).

24. Fidler, I.J. The pathogenesis of cancer metastasis: the'seed and soil'hypothesis revisited. *Nature Reviews Cancer* **3**, 453 (2003).

25. Bogenrieder, T. & Herlyn, M. Axis of evil: molecular mechanisms of cancer metastasis. *Oncogene* **22**, 6524 (2003).

26. Chaffer, C.L., San Juan, B.P., Lim, E. & Weinberg, R.A. EMT, cell plasticity and metastasis. *Cancer and Metastasis Reviews* **35**, 645-654 (2016).

27. Kalluri, R. EMT: when epithelial cells decide to become mesenchymal-like cells. *The Journal of clinical investigation* **119**, 1417-1419 (2009).

28. Vincan, E. & Barker, N. The upstream components of the Wnt signalling pathway in the dynamic EMT and MET associated with colorectal cancer progression. *Clinical & experimental metastasis* **25**, 657-663 (2008).

29. Willis, B.C. & Borok, Z. TGF-β-induced EMT: mechanisms and implications for fibrotic lung disease. *American Journal of Physiology-Lung Cellular and Molecular Physiology* **293**, L525-L534 (2007).

30. Wang, Z., Li, Y., Kong, D. & H Sarkar, F. The role of Notch signaling pathway in epithelial-mesenchymal transition (EMT) during development and tumor aggressiveness. *Current drug targets* **11**, 745-751 (2010).

31. Kotiyal, S. & Bhattacharya, S. Breast cancer stem cells, EMT and therapeutic targets. *Biochemical and biophysical research communications* **453**, 112-116 (2014).

32. Puisieux, A., Brabletz, T. & Caramel, J. Oncogenic roles of EMT-inducing transcription factors. *Nature cell biology* **16**, 488 (2014).

33. Sánchez-Tilló, E., Liu, Y., de Barrios, O., Siles, L., Fanlo, L., Cuatrecasas, M., Darling, D.S., Dean, D.C., Castells, A. & Postigo, A. EMT-activating transcription factors in cancer: beyond EMT and tumor invasiveness. *Cellular and molecular life sciences* **69**, 3429-3456 (2012).

34. Batlle, E., Sancho, E., Franci, C., Dominguez, D., Monfar, M., Baulida, J. & Garcia De Herreros, A. The transcription factor snail is a repressor of E-cadherin gene expression in epithelial tumour cells. *Nat Cell Biol* **2**, 84-89 (2000).

35. Yang, J., Mani, S.A., Donaher, J.L., Ramaswamy, S., Itzykson, R.A., Come, C., Savagner, P., Gitelman, I., Richardson, A. & Weinberg, R.A. Twist, a master regulator of morphogenesis, plays an essential role in tumor metastasis. *Cell* **117**, 927-939 (2004).

36. Cavallaro, U. & Christofori, G. Cell adhesion and signalling by cadherins and Ig-CAMs in cancer. *Nature Reviews Cancer* **4**, 118 (2004).

37. Oka, H., Shiozaki, H., Kobayashi, K., Inoue, M., Tahara, H., Kobayashi, T., Takatsuka, Y., Matsuyoshi, N., Hirano, S. & Takeichi, M. Expression of E-cadherin cell adhesion molecules in human breast cancer tissues and its relationship to metastasis. *Cancer research* **53**, 1696-1701 (1993).

38. Baranwal, S. & Alahari, S.K. Molecular mechanisms controlling E-cadherin expression in breast cancer. *Biochemical and biophysical research communications* **384**, 6-11 (2009).

39. Rakha, E.A., El-Sayed, M.E., Green, A.R., Lee, A.H., Robertson, J.F. & Ellis, I.O. Prognostic markers in triple-negative breast cancer. *Cancer* **109**, 25-32 (2007).

40. Thompson, E.W., Paik, S., Brünner, N., Sommers, C.L., Zugmaier, G., Clarke, R., Shima, T.B., Torri, J., Donahue, S. & Lippman, M.E. Association of increased basement membrane invasiveness with absence of estrogen receptor and expression of vimentin in human breast cancer cell lines. *Journal of cellular physiology* **150**, 534-544 (1992).

41. Vuoriluoto, K., Haugen, H., Kiviluoto, S., Mpindi, J., Nevo, J., Gjerdrum, C., Tiron, C., Lorens, J. & Ivaska, J. Vimentin regulates EMT induction by Slug and oncogenic H-Ras and migration by governing Axl expression in breast cancer. *Oncogene* **30**, 1436 (2011).

42. Singh, A. & Settleman, J. EMT, cancer stem cells and drug resistance: an emerging axis of evil in the war on cancer. *Oncogene* **29**, 4741 (2010).

43. Polyak, K. & Weinberg, R.A. Transitions between epithelial and mesenchymal states: acquisition of malignant and stem cell traits. *Nature Reviews Cancer* **9**, 265 (2009).

44. Batlle, E. & Clevers, H. Cancer stem cells revisited. *Nature medicine* **23**, 1124 (2017).

45. Maycas, M., Esbrit, P. & Gortazar, A.R. Molecular mechanisms in bone mechanotransduction. *Histology and histopathology* **32**, 751-760 (2017).

46. Sikavitsas, V.I., Temenoff, J.S. & Mikos, A.G. Biomaterials and bone mechanotransduction. *Biomaterials* **22**, 2581-2593 (2001).

47. Hahn, C. & Schwartz, M.A. Mechanotransduction in vascular physiology and atherogenesis. *Nature reviews Molecular cell biology* **10**, 53 (2009).

48. Huang, S. & Ingber, D.E. Cell tension, matrix mechanics, and cancer development. *Cancer cell* **8**, 175-176 (2005).

49. Seewaldt, V. ECM stiffness paves the way for tumor cells. *Nature medicine* **20**, 332 (2014).

50. Pathak, A. & Kumar, S. Biophysical regulation of tumor cell invasion: moving beyond matrix stiffness. *Integrative Biology* **3**, 267-278 (2011).

51. Engler, A.J., Sen, S., Sweeney, H.L. & Discher, D.E. Matrix elasticity directs stem cell lineage specification. *Cell* **126**, 677-689 (2006).

52. Heppner, K.J., Matrisian, L.M., Jensen, R.A. & Rodgers, W.H. Expression of most matrix metalloproteinase family members in breast cancer represents a tumor-induced host response. *The American journal of pathology* **149**, 273 (1996).

53. Ramaswamy, S., Ross, K.N., Lander, E.S. & Golub, T.R. A molecular signature of metastasis in primary solid tumors. *Nature genetics* **33**, 49 (2002).

54. Oskarsson, T. Extracellular matrix components in breast cancer progression and metastasis. *The Breast* **22**, S66-S72 (2013).

55. Colpaert, C., Vermeulen, P., Van Marck, E. & Dirix, L. The presence of a fibrotic focus is an independent predictor of early metastasis in lymph node-negative breast cancer patients. *The American journal of surgical pathology* **25**, 1557-1558 (2001).

56. Conklin, M.W., Eickhoff, J.C., Riching, K.M., Pehlke, C.A., Eliceiri, K.W., Provenzano, P.P., Friedl, A. & Keely, P.J. Aligned collagen is a prognostic signature for survival in human breast carcinoma. *Am J Pathol* **178**, 1221-1232 (2011).

57. Kirschmann, D.A., Seftor, E.A., Fong, S.F., Nieva, D.R., Sullivan, C.M., Edwards, E.M., Sommer, P., Csiszar, K. & Hendrix, M.J. A molecular role for lysyl oxidase in breast cancer invasion. *Cancer research* **62**, 4478-4483 (2002).

58. Ioachim, E., Charchanti, A., Briasoulis, E., Karavasilis, V., Tsanou, H., Arvanitis, D., Agnantis, N.J. & Pavlidis, N. Immunohistochemical expression of extracellular matrix components tenascin, fibronectin, collagen type IV and laminin in breast cancer: their prognostic value and role in tumour invasion and progression. *European journal of cancer* **38**, 2362-2370 (2002).

59. Auvinen, P., Tammi, R., Parkkinen, J., Tammi, M., Ågren, U., Johansson, R., Hirvikoski, P., Eskelinen, M. & Kosma, V.-M. Hyaluronan in peritumoral stroma and malignant cells associates with breast cancer spreading and predicts survival. *The American journal of pathology* **156**, 529-536 (2000).

60. Levental, K.R., Yu, H., Kass, L., Lakins, J.N., Egeblad, M., Erler, J.T., Fong, S.F., Csiszar, K., Giaccia, A. & Weninger, W. Matrix crosslinking forces tumor progression by enhancing integrin signaling. *Cell* **139**, 891-906 (2009).

61. Lu, P., Weaver, V.M. & Werb, Z. The extracellular matrix: a dynamic niche in cancer progression. *The Journal of cell biology* **196**, 395-406 (2012).

62. Wei, S.C., Fattet, L., Tsai, J.H., Guo, Y., Pai, V.H., Majeski, H.E., Chen, A.C., Sah, R.L., Taylor, S.S. & Engler, A.J. Matrix stiffness drives epithelial–mesenchymal transition and tumour metastasis through a TWIST1–G3BP2 mechanotransduction pathway. *Nature cell biology* **17**, 678 (2015).

63. Dobrokhotov, O., Samsonov, M., Sokabe, M. & Hirata, H. Mechanoregulation and pathology of YAP/TAZ via Hippo and non-Hippo mechanisms. *Clinical and translational medicine* **7**, 23 (2018).

64. Meng, Z., Qiu, Y., Lin, K.C., Kumar, A., Placone, J.K., Fang, C., Wang, K.C., Lu, S., Pan, M., Hong, A.W., Moroishi, T., Luo, M., Plouffe, S.W., Diao, Y., Ye, Z., Park, H.W., Wang, X., Yu, F.X., Chien, S., Wang, C.Y., Ren, B., Engler, A.J. & Guan, K.L. RAP2 mediates mechanoresponses of the Hippo pathway. *Nature* **560**, 655-660 (2018).

65. Lo, C.M., Wang, H.B., Dembo, M. & Wang, Y.L. Cell movement is guided by the rigidity of the substrate. *Biophysical journal* **79**, 144-152 (2000).

66. Yeung, T., Georges, P.C., Flanagan, L.A., Marg, B., Ortiz, M., Funaki, M., Zahir, N., Ming, W., Weaver, V. & Janmey, P.A. Effects of substrate stiffness on cell morphology, cytoskeletal structure, and adhesion. *Cell motility and the cytoskeleton* **60**, 24-34 (2005).

67. Happe, C.L., Tenerelli, K.P., Gromova, A.K., Kolb, F. & Engler, A.J. Mechanically patterned neuromuscular junctions-in-a-dish have improved functional maturation. *Molecular biology of the cell* **28**, 1950-1958 (2017).

68. Choi, Y.S., Vincent, L.G., Lee, A.R., Kretchmer, K.C., Chirasatitsin, S., Dobke, M.K. & Engler, A.J. The alignment and fusion assembly of adipose-derived stem cells on mechanically patterned matrices. *Biomaterials* **33**, 6943-6951 (2012).

69. Rowlands, A.S., George, P.A. & Cooper-White, J.J. Directing osteogenic and myogenic differentiation of MSCs: interplay of stiffness and adhesive ligand presentation. *American journal of physiology. Cell physiology* **295**, C1037-1044 (2008).

70. Khatiwala, C.B., Peyton, S.R. & Putnam, A.J. Intrinsic mechanical properties of the extracellular matrix affect the behavior of pre-osteoblastic MC3T3-E1 cells. *American journal of physiology. Cell physiology* **290**, C1640-1650 (2006).

71. Ng, M.R. & Brugge, J.S. A stiff blow from the stroma: collagen crosslinking drives tumor progression. *Cancer cell* **16**, 455-457 (2009).

72. Williams, C.M., Engler, A.J., Slone, R.D., Galante, L.L. & Schwarzbauer, J.E. Fibronectin expression modulates mammary epithelial cell proliferation during acinar differentiation. *Cancer research* **68**, 3185-3192 (2008).

73. Saulnier, R., Bhardwaj, B., Klassen, J., Leopold, D., Rahimi, N., Tremblay, E., Mosher, D. & Elliott, B. Fibronectin fibrils and growth factors stimulate anchorage-independent growth of a murine mammary carcinoma. *Experimental cell research* **222**, 360-369 (1996).

74. Kao, R.T., Hall, J., Engel, L. & Stern, R. The matrix of human breast tumor cells is mitogenic for fibroblasts. *The American journal of pathology* **115**, 109-116 (1984).

75. Ishihara, S., Inman, D.R., Li, W.J., Ponik, S.M. & Keely, P.J. Mechano-Signal Transduction in Mesenchymal Stem Cells Induces Prosaposin Secretion to Drive the Proliferation of Breast Cancer Cells. *Cancer research* **77**, 6179-6189 (2017).

76. Affo, S., Yu, L.X. & Schwabe, R.F. The Role of Cancer-Associated Fibroblasts and Fibrosis in Liver Cancer. *Annual review of pathology* **12**, 153-186 (2017).

77. Pankova, D., Chen, Y., Terajima, M., Schliekelman, M.J., Baird, B.N., Fahrenholtz, M., Sun, L., Gill, B.J., Vadakkan, T.J., Kim, M.P., Ahn, Y.H., Roybal, J.D., Liu, X., Parra Cuentas, E.R., Rodriguez, J., Wistuba, II, Creighton, C.J., Gibbons, D.L., Hicks, J.M., Dickinson, M.E., West, J.L., Grande-Allen, K.J., Hanash, S.M., Yamauchi, M. & Kurie, J.M. Cancer-Associated Fibroblasts Induce a Collagen Cross-link Switch in Tumor Stroma. *Molecular cancer research : MCR* **14**, 287-295 (2016).

78. Wang, K., Andresen Eguiluz, R.C., Wu, F., Seo, B.R., Fischbach, C. & Gourdon, D. Stiffening and unfolding of early deposited-fibronectin increase proangiogenic factor secretion by breast cancer-associated stromal cells. *Biomaterials* **54**, 63-71 (2015).

79. Wei, S.C., Fattet, L., Tsai, J.H., Guo, Y., Pai, V.H., Majeski, H.E., Chen, A.C., Sah, R.L., Taylor, S.S. & Engler, A.J. Matrix stiffness drives epithelial-mesenchymal transition and tumour metastasis through a TWIST1-G3BP2 mechanotransduction pathway. *Nature cell biology* **17**, 678 (2015).

80. Alonso-Nocelo, M., Raimondo, T.M., Vining, K.H., Lopez-Lopez, R., de la Fuente, M. & Mooney, D.J. Matrix stiffness and tumor-associated macrophages modulate epithelial to mesenchymal transition of human adenocarcinoma cells. *Biofabrication* **10**, 035004 (2018).

81. Berg, W.A., Cosgrove, D.O., Dore, C.J., Schafer, F.K., Svensson, W.E., Hooley, R.J., Ohlinger, R., Mendelson, E.B., Balu-Maestro, C., Locatelli, M., Tourasse, C., Cavanaugh, B.C., Juhan, V., Stavros, A.T., Tardivon, A., Gay, J., Henry, J.P. & Cohen-Bacrie, C. Shear-wave elastography improves the specificity of breast US: the BE1 multinational study of 939 masses. *Radiology* **262**, 435-449 (2012).

82. Burdick, J.A. & Murphy, W.L. Moving from static to dynamic complexity in hydrogel design. *Nature communications* **3**, 1269 (2012).

83. Stowers, R.S., Allen, S. C., Sanchez, K., Davis, C. L., Ebelt, N. D., Van Den Berg, C. & Suggs, L. J. Extracellular matrix stiffening induces a malignant phenotypic transition in breast epithelial cells. *Cell. Mol. Bioeng.* **10**, 114-123 (2017).

84. Masuike, T., Taki, S., Hara, K. & Kai, S. Change of Temperature and Elastic Stiffness during Dehydration Process of Polyacrylamide Gel. *Jpn. J. Appl. Phys.* **34**, 4997–5000 (1995).

85. Guvendiren, M. & Burdick, J.A. Stiffening hydrogels to probe short- and long-term cellular responses to dynamic mechanics. *Nature communications* **3**, 792 (2012).

86. Caliari, S.R., Perepelyuk, M., Cosgrove, B.D., Tsai, S.J., Lee, G.Y., Mauck, R.L., Wells, R.G. & Burdick, J.A. Stiffening hydrogels for investigating the dynamics of hepatic stellate cell mechanotransduction during myofibroblast activation. *Scientific reports* **6**, 21387 (2016).

87. Burdick, J.A., Chung, C., Jia, X., Randolph, M.A. & Langer, R. Controlled degradation and mechanical behavior of photopolymerized hyaluronic acid networks. *Biomacromolecules* **6**, 386-391 (2005).

88. Marklein, R.A.B., J. A. Spatially controlled hydrogel mechanics to modulate stem cell interactions. *Soft Matter* **6**, 386–391 (2009).

89. Kloxin, A.M., Kasko, A.M., Salinas, C.N. & Anseth, K.S. Photodegradable hydrogels for dynamic tuning of physical and chemical properties. *Science* **324**, 59-63 (2009).

90. Tse, J.R. & Engler, A.J. Stiffness gradients mimicking in vivo tissue variation regulate mesenchymal stem cell fate. *PLoS One* **6**, e15978 (2011).

91. Nasrollahi, S., Walter, C., Loza, A.J., Schimizzi, G.V., Longmore, G.D. & Pathak, A. Past matrix stiffness primes epithelial cells and regulates their future collective migration through a mechanical memory. *Biomaterials* **146**, 146-155 (2017).

92. Ondeck, M.G. & Engler, A.J. Mechanical Characterization of a Dynamic and Tunable Methacrylated Hyaluronic Acid Hydrogel. *Journal of biomechanical engineering* **138**, 021003 (2016).

93. Wen, J.H., Vincent, L.G., Fuhrmann, A., Choi, Y.S., Hribar, K.C., Taylor-Weiner, H., Chen, S. & Engler, A.J. Interplay of matrix stiffness and protein tethering in stem cell differentiation. *Nature materials* **13**, 979-987 (2014).

94. Dupont, S., Morsut, L., Aragona, M., Enzo, E., Giulitti, S., Cordenonsi, M., Zanconato, F., Le Digabel, J., Forcato, M., Bicciato, S., Elvassore, N. & Piccolo, S. Role of YAP/TAZ in mechanotransduction. *Nature* **474**, 179-183 (2011).

95. Panciera, T., Azzolin, L., Cordenonsi, M. & Piccolo, S. Mechanobiology of YAP and TAZ in physiology and disease. *Nature reviews. Molecular cell biology* **18**, 758-770 (2017).

96. Kaukonen, R., Mai, A., Georgiadou, M., Saari, M., De Franceschi, N., Betz, T., Sihto, H., Ventela, S., Elo, L., Jokitalo, E., Westermarck, J., Kellokumpu-Lehtinen, P.L., Joensuu, H., Grenman, R. & Ivaska, J. Normal stroma suppresses cancer cell proliferation via mechanosensitive regulation of JMJD1a-mediated transcription. *Nature communications* **7**, 12237 (2016).

97. Young, J.L., Kretchmer, K., Ondeck, M.G., Zambon, A.C. & Engler, A.J. Mechanosensitive kinases regulate stiffness-induced cardiomyocyte maturation. *Scientific reports* **4**, 6425 (2014).

98. Kiang, J.D., Wen, J.H., del Alamo, J.C. & Engler, A.J. Dynamic and reversible surface topography influences cell morphology. *Journal of biomedical materials research. Part A* **101**, 2313-2321 (2013).

99. Yousaf, M.N., Houseman, B.T. & Mrksich, M. Turning On Cell Migration with Electroactive Substrates *Angewandte Chemie (International ed. in English)* **40**, 1093-1096 (2001).

100. Gillette, B.M., Jensen, J.A., Wang, M., Tchao, J. & Sia, S.K. Dynamic hydrogels: switching of 3D microenvironments using two-component naturally derived extracellular matrices. *Advanced materials (Deerfield Beach, Fla.)* **22**, 686-691 (2010).

101. Alizadeh, A.A., Aranda, V., Bardelli, A., Blanpain, C., Bock, C., Borowski, C., Caldas, C., Califano, A., Doherty, M. & Elsner, M. Toward understanding and exploiting tumor heterogeneity. *Nature medicine* **21**, 846 (2015).

102. Shipitsin, M., Campbell, L.L., Argani, P., Weremowicz, S., Bloushtain-Qimron, N., Yao, J., Nikolskaya, T., Serebryiskaya, T., Beroukhim, R. & Hu, M. Molecular definition of breast tumor heterogeneity. *Cancer cell* **11**, 259-273 (2007).

103. Tse, J.R. & Engler, A.J. Preparation of hydrogel substrates with tunable mechanical properties. *Current protocols in cell biology* **Chapter 10**, Unit 10.16 (2010).